the plant journal

SEB SOCIETY FOR EXPERIMENTAL BIOLOGY

*The Plant Journal* (2020) **102,** 34–52 doi: 10.1111/tpj.14610

# Intertwined metal homeostasis, oxidative and biotic stress responses in the Arabidopsis *frd3* mutant

**Maxime Scheepers[1], Julien Spielmann[1], Madeleine Boulanger[2,3], Monique Carnol[4], Bernard Bosman[4], Edwin De Pauw[2], Erik Goormaghtigh[5], Patrick Motte[1] and Marc Hanikenne[1,*]**

[1]*InBioS-PhytoSystems, Functional Genomics and Plant Molecular Imaging, University of Liège, 4000 Liège, Belgium,*
[2]*Laboratory of Mass Spectrometry, Departement of Chemistry, University of Liège, 4000 Liège, Belgium,*
[3]*InBioS-Center for Protein Engineering (CIP), Bacterial Physiology and Genetics, University of Liège, 4000 Liège, Belgium,*
[4]*InBioS-PhytoSystems, Laboratory of Plant and Microbial Ecology, University of Liège, 4000 Liège, Belgium, and*
[5]*Structure and Function of Biological membranes, Center for Structural Biology and Bioinformatics, Université Libre de Bruxelles, 1050 Brussels, Belgium*

Received 21 August 2018; revised 24 October 2019; accepted 31 October 2019; published online 13 November 2019.
*For correspondence (e-mail: marc.hanikenne@uliege.be)

## SUMMARY

**FRD3 (FERRIC REDUCTASE DEFECTIVE 3) plays a major role in iron (Fe) and zinc (Zn) homeostasis in Arabidopsis. It transports citrate, which enables metal distribution in the plant. An *frd3* mutant is dwarf and chlorotic and displays a constitutive Fe-deficiency response and strongly altered metal distribution in tissues. Here, we have examined the interaction between Fe and Zn homeostasis in an *frd3* mutant exposed to varying Zn supply. Detailed phenotyping using transcriptomic, ionomic, histochemical and spectroscopic approaches revealed the full complexity of the *frd3* mutant phenotype, which resulted from altered transition metal homeostasis, manganese toxicity, and oxidative and biotic stress responses. The cell wall played a key role in these processes, as a site for Fe and hydrogen peroxide accumulation, and displayed modified structure in the mutant. Finally, we showed that Zn excess interfered with these mechanisms and partially restored root growth of the mutant, without reverting the Fe-deficiency response. In conclusion, the *frd3* mutant molecular phenotype is more complex than previously described and illustrates how the response to metal imbalance depends on multiple signaling pathways.**

**Keywords: ferric chelate reductase 3, FRD3, zinc, iron, manganese, Arabidopsis, biotic defense, oxidative stress, homeostasis crosstalk.**

## INTRODUCTION

Iron (Fe) is an essential micronutrient for plant growth and quality (Briat *et al.*, 2015) and for human health (World Health Organization, WHO; http://www.who.int/nutrition/en/). Fe is one of the five most abundant metals in soils but it is barely accessible to plants as it is highly insoluble, especially in alkaline soils (Marschner and Marschner, 2012). As plants are at the base of the food pyramid, Fe deficiency is the most common human nutritional disorder, with approximatively 30% of the world population affected by anemia (WHO; http://www.who.int/nutrition/en/).

In plant cells, Fe is involved in numerous redox processes. As a component of heme and Fe–sulfur clusters, it is a major cofactor for both the respiratory electron transfer chain (Palmer and Guerinot, 2009; Nouet *et al.*, 2011) and photosynthesis (Hanikenne *et al.*, 2014). It is, for instance, required for chlorophyll synthesis (Kobayashi and Nishizawa, 2012). Fe also participates in several important processes, such as root morphology, flower and pollen development, nutrient assimilation (e.g. sulfate) and hormone biosynthesis (e.g. ethylene) (Bouzayen *et al.*, 1991; Schmidt, 1999; Takahashi *et al.*, 2003). In addition to these essential roles, Fe can also be cytotoxic. As a redox-active metal, excess Fe can trigger the formation of reactive oxygen species (ROS) (Stohs and Bagchi, 1995; Marschner and Marschner, 2012).

Plants have developed mechanisms to efficiently take up Fe from the soil (Walker and Connolly, 2008). Dicotyledonous and non-graminaceous monocotyledonous plants use Fe-uptake machinery, termed strategy I, based on the reduction of $Fe^{3+}$ to $Fe^{2+}$ (Römheld, 1987). In contrast, grasses use strategy II, based on $Fe^{3+}$ chelation and uptake from the soil (Schmidt, 2003). In Arabidopsis, ARABIDOPSIS $H^+$-ATPase 2 (AHA2) is responsible for the first step of

strategy I, consisting of proton pumping into the rhizosphere (Santi and Schmidt, 2009), resulting in local acidification that increases $Fe^{3+}$ solubility (Guerinot and Yi, 1994). $Fe^{3+}$ is then reduced to $Fe^{2+}$ by the plasma membrane-bound enzyme FERRIC REDUCTASE-OXIDASE 2 (FRO2) (Robinson *et al.*, 1999). $Fe^{2+}$ is finally taken up at the plasmamembrane of the root epidermis cells by IRON-REGULATED TRANSPORTER 1 (IRT1), a member of the ZRT-IRT-LIKE PROTEIN (ZIP) family. IRT1 has a high affinity for $Fe^{2+}$ but also for a range of divalent metal cations, including $Zn^{2+}$, $Mn^{2+}$, $Ni^{2+}$ and also $Cd^{2+}$ (Eide *et al.*, 1996; Vert *et al.*, 2002). Moreover, the secretion of phenolic compounds was recently shown to increase the availability of $Fe^{3+}$. The F6-H1 (a coumarin biosynthesis enzyme) and ATP-BINDING CASSETTE G37 (ABCG37), also called PLEIOTROPIC DRUG RESISTANCE 9 (PDR9), proteins are involved in the synthesis and secretion, respectively, of phenolics by the roots (Fourcroy *et al.*, 2014; Schmidt *et al.*, 2014).

The regulation of Fe uptake and the Fe-deficiency response in Arabidopsis is complex and notably controlled by the transcription factor FER-LIKE IRON-DEFICIENCY-INDUCED TRANSCRIPTION FACTOR (FIT), which is required for the upregulation in the expression of, among others, the *AHA2*, *FRO2*, *IRT1*, *F6H1* and *ABCG37* genes under Fe deficiency (Colangelo and Guerinot, 2004; Yuan *et al.*, 2005; Ivanov *et al.*, 2012; Rodríguez-Celma *et al.*, 2013; Schmidt *et al.*, 2014). FIT is a BASIC HELIX-LOOP-HELIX (bHLH) protein, and needs interaction with an additional bHLH protein (bHLH038, 039, 100 or 101) to activate the strategy-I response (Yuan *et al.*, 2008). BRUTUS (BTS), an E3-ligase, is also able to interact with different bHLHs (bHLH034, 104 and 105) to control the transcription of the *bHLH038*, *039*, *100* and *101* genes in response to Fe availability, whereas two BTS-like proteins were recently shown to directly interact with and regulate FIT (Rodríguez-Celma *et al.*, 2019). The BTS–bHLH complex also regulates POPEYE (PYE), which negatively controls genes involved in iron mobility between roots and shoots (Long *et al.*, 2010; Li *et al.*, 2016). Two proteins of the MYELOBLASTOSIS (MYB) transcription factor family (MYB10 and MYB72) are also involved in the Fe-deficiency response and regulate *NICOTINAMINE SYNTHASE 4* (*NAS4*) (Sivitz *et al.*, 2012; Palmer *et al.*, 2013; Brumbarova *et al.*, 2015).

Once inside the roots, Fe is transported symplastically, mostly chelated by nicotianamine (NA), and apoplastically to vascular tissues, where it is possibly loaded into the xylem by FERROPORTIN 1 (FPN1), also called IRON REGULATED 1 (IREG1), for root-to-shoot translocation (Morrissey *et al.*, 2009). In the xylem, Fe is unable to move freely and is chelated essentially by citrate (Rellán-Álvarez *et al.*, 2010). Citrate, an organic acid, is essential for the proper mobility and distribution of Fe in roots, shoots, anthers, pollen and seeds (Roschzttardtz *et al.*, 2011). *FERRIC REDUCTASE DEFFECTIVE 3* (*FRD3*) encodes a plasma membrane transporter expressed in the root pericycle in Arabidopsis and is involved in citrate efflux into the xylem. FRD3 plays a key role in Fe homeostasis (Rogers and Guerinot, 2002; Green and Rogers, 2004; Durrett *et al.*, 2007). In an *frd3* mutant (allelic to *MANGANESE ACCUMULATOR 1*, *man-1*; Delhaize, 1996), a 40% reduction of citrate levels in the xylem sap is associated with leaf chlorosis, plant growth reduction and Fe accumulation in the root vascular tissues (Rogers and Guerinot, 2002; Green and Rogers, 2004; Durrett *et al.*, 2007). Furthermore, *frd3* plants express constitutively the Fe-deficiency response, including *IRT1*, and consequently accumulate high levels of manganese (Mn), zinc (Zn) and Fe in roots and shoots (Delhaize, 1996; Rogers and Guerinot, 2002; Green and Rogers, 2004).

Secondary Fe deficiency is typically a major component of Zn excess toxicity. Increased Fe supply indeed alleviates Zn toxicity symptoms in Arabidopsis (Shanmugam *et al.*, 2011). In addition to its major role in Fe homeostasis, FRD3 also contributes to the interaction between Fe and Zn homeostasis. A quantitative trait locus analysis identified *FRD3* as a determinant of variation in Zn tolerance among Arabidopsis ecotypes. A higher expression of *FRD3* in response to Zn excess was co-segregating with higher Zn tolerance and reduced impact of Zn excess on Fe homeostasis (Pineau *et al.*, 2012). Moreover, the two *FRD3* transcript variants undergo differential expression and translation efficiencies upon Zn excess (Charlier *et al.*, 2015).

In this study, we assessed the response of an Arabidopsis *frd3* mutant (*frd3*-7) to varying Zn supply to examine the connection between Fe and Zn homeostasis. We show that the dwarfed phenotype of the mutant in normal growth conditions results from multiple alterations in Fe, Mn and Zn homeostasis, as well as in cell walls and in oxidative and biotic stress responses. Exposure to higher Zn concentrations reverted most of these phenotypes in roots. Our results highlight that the response to metal homeostasis imbalance is intertwined with multiple signaling pathways.

## RESULTS

### Altered Zn phenotype of the *frd3* mutant

When grown hydroponically under control conditions (1 μM Zn), the *frd3* mutant was small and chlorotic compared with the wild-type (WT, Col-0) (Figures 1 and S1), as previously described (Rogers and Guerinot, 2002). The root growth phenotype was partially rescued when Zn supply was increased to 5 and 20 μM (Figure 1a,b). When exposed to 20 μM Zn, root growth more than doubled compared with the control, although shoots remained small and

chlorotic compared with the WT (Figures 1c,d, S1). Similar results were obtained with seedlings grown *in vitro* (Figure S2). The *frd3* mutant displayed a 40% reduction in root growth compared with the WT under control conditions. Upon exposure to high levels of Zn (75 μM Zn), root growth in the WT was reduced by 30%, whereas root growth was slightly but significantly increased in the *frd3* mutant. At high levels of Zn there were no differences between root growth in the WT and the *frd3* mutant (Figure S2a). The *frd3* shoots remained smaller than in the WT at high levels of Zn, similar to observations in hydropony (Figures 1d and S2b).

**Impact of Zn on the mobilization of Fe and Zn in the *frd3* mutant**

Next, the impact of exposure to high levels of Zn on the typical metal accumulation phenotypes of the *frd3* mutant was examined. When grown hydroponically under control conditions (1 μM Zn), the *frd3* mutant accumulated more Fe, Zn and Mn (6-, 7- and 22-fold, respectively) in the roots than the WT (Figure 2a). The mutant also accumulated more Zn and Mn in the shoots (3.5- and 4.0-fold, respectively) (Figure S3), as described previously (Delhaize, 1996; Rogers and Guerinot, 2002). Upon exposure to high levels

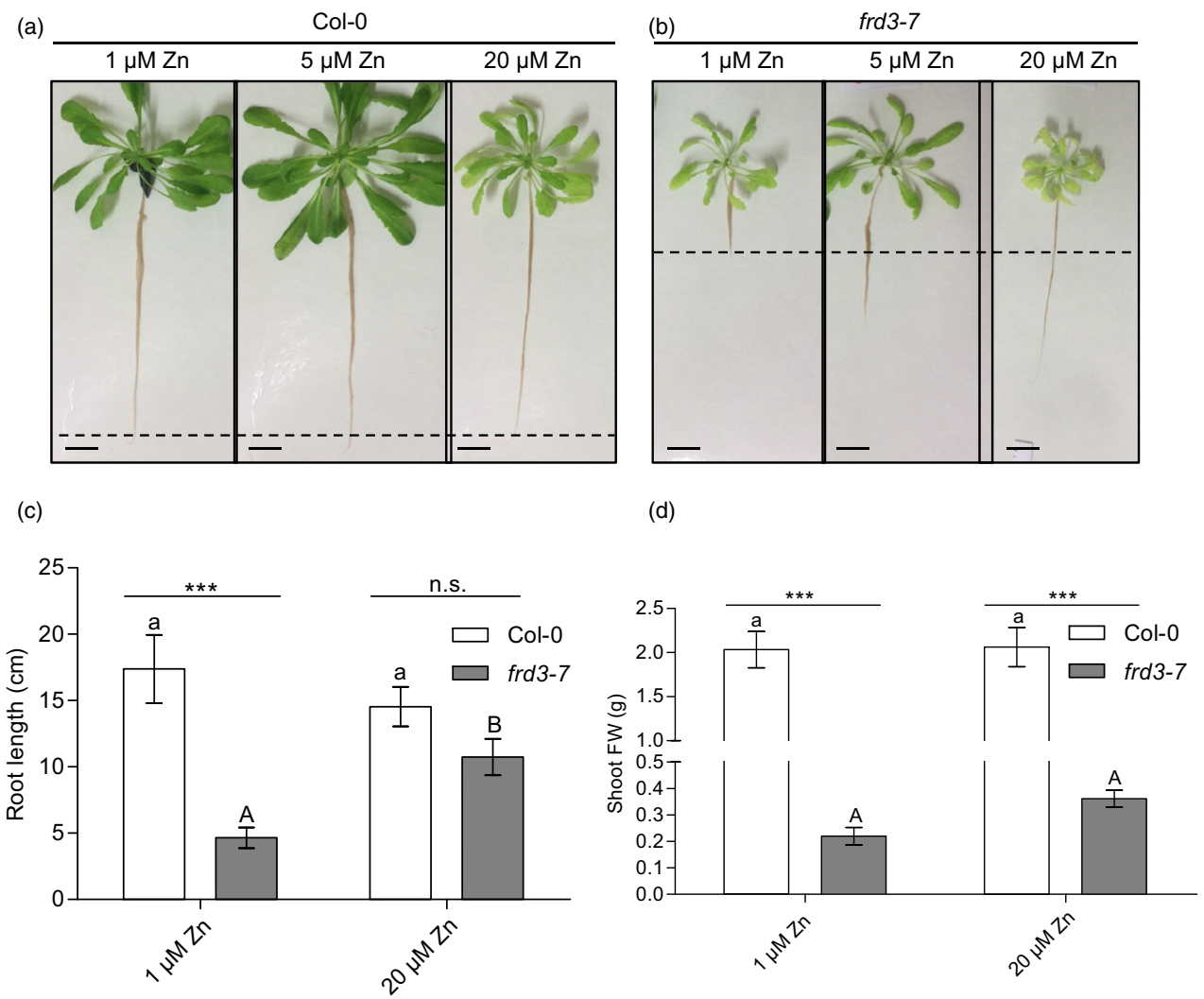


**Figure 1.** Impact of Zn on growth phenotypes. (a) Col-0 and (b) *frd3-7* plant phenotypes upon growth in hydropony and exposure to different concentrations of Zn (1, 5 and 20 μM $ZnSO_4$). Dotted bars mark the root length of Col-0 (a) or *frd3-7* (b) grown in control conditions (1 μM $ZnSO_4$). Scale bars: 2.5 cm. The pictures are representative of three independent experiments each including six plants per genotype and growing conditions. (c) Root growth and (d) shoot fresh weight (FW) of Col-0 (white) and *frd3-7* (grey) plants grown at 1 and 20 μM $ZnSO_4$. Data represent mean values (± SEMs) of three independent experiments, each including six plants per genotype and growing conditions. The data were analyzed by two-way ANOVA followed by Bonferroni's multiple-comparison post-hoc test. Statistically significant differences between means are indicated by asterisks (within conditions, ***$P < 0.001$, n.s. not significant) or different letters (within genotypes, $P < 0.05$).

of Zn (20 μM Zn) the concentrations of Zn were similar in the roots and shoots of both the mutant and the WT, as a result of increased Zn accumulation in the WT. The impact on Fe accumulation in the mutant was limited, with a slight decrease of Fe concentrations in both the roots and the shoots. In contrast, Zn exposure drastically reduced Mn accumulation in the mutant (by approximately 97% in the roots and 69% in shoots). The ionomic profile of plants exposed to 5 μM Zn was more or less intermediate between plants grown under control and 20 μM Zn conditions (Figures 2a and S3).

A typical phenotype of the *frd3* mutant is the accumulation of $Fe^{3+}$ in the root vascular tissues, which can be visualized by Perls staining and enhanced by diaminobenzidine (DAB) (Green and Rogers, 2004; Roschzttardtz *et al.*, 2011). Accordingly, a positive staining was observed in roots and root sections of the *frd3* mutant under control conditions (Figure 2b). With 20 μM Zn the staining was no longer observed in *frd3* roots, suggesting competition between Fe and Zn in roots upon exposure to high levels of Zn (Figure 2b). No staining was observed in mutant and WT shoots. Note that exposure to high levels of Zn (75 μM Zn) had similar effects on both the ionome and Fe accumulation in the vascular tissues of seedlings grown *in vitro* (Figure S4).

Finally, Zn distribution in WT and *frd3* roots was imaged using the Zn fluorophore Zinpyr-1 (Sinclair *et al.*, 2007) (Figure 2c). In WT roots, the Zn-associated green fluorescence was localized in the vascular bundle. In the *frd3* mutant, massive Zn accumulation was observed in some endodermis cells in addition to vascular tissues. Upon exposure to high levels of Zn, the fluorescence of the Zn–Zinpyr-1 complex was only observed in the root vascular tissues of both genotypes, with a higher intensity compared with plants grown under control conditions.

Metal distribution in the *frd3* root was dependent on the Fe and Zn concentration ratio of the medium (Figure S5). When the Fe/Zn concentration ratio in the medium was lower or equal to 1, typical *frd3* phenotypes were no longer observed, with no $Fe^{3+}$ staining in the mutant root, as described in Figure 2. Conversely, when this ratio was higher than 1, $Fe^{3+}$ staining was observed in *frd3* roots.

### Mn toxicity in the *frd3* mutant

A particularly striking phenotype of the *frd3* mutant is the massive accumulation of Mn in root and shoot tissues under control conditions, and its almost complete reversal upon exposure to high levels of Zn (Figures 2a and S3). Next we examined whether Mn accumulation contributed to the *frd3* mutant phenotype. Both WT and mutant plants were grown under control conditions (5 μM Mn) and at Mn deficiency (0 μM Mn) (Figure 3). The treatment abolished Mn accumulation in root and shoot tissues of the *frd3* mutant (Figure S6a,b). Mn deficiency slightly decreased root growth in the WT, whereas by contrast it increased root growth in the *frd3* mutant (by approximately 33%) compared with control conditions. Consequently, no growth difference was observed between the WT and the mutant under Mn deficiency (Figure 3a). This condition had no influence on $Fe^{3+}$ accumulation in the mutant root vascular tissues (Figure 3b).

Combined Mn deficiency (0 μM Mn) and exposure to high levels of Zn (75 μM Zn) restored root growth in the *frd3* mutant, similar to Mn deficiency alone (Figure 3a), and resulted in competition between Fe and Zn in the mutant root, similar to Zn excess alone (Figure 3b). Note that Mn deficiency had a limited impact on *frd3* shoot growth (Figure S6c). Altogether, these observations suggest that Mn accumulation resulted in toxicity in the *frd3* mutant, and was at least partly responsible for its altered root growth, but did not influence the Fe-related phenotypes of the mutant (e.g. accumulation of $Fe^{3+}$ in the root).

### Transcriptome profiling of the *frd3* mutant

To shed light on the molecular mechanisms underlying the complex interplay between Fe, Zn and Mn observed in the *frd3* mutant roots, a transcriptomic profiling of root tissues of WT and *frd3* plants grown under control conditions (1 μM Zn) and under Zn excess (20 μM Zn) was conducted using RNA-Seq. Principal component analysis (PCA) revealed that PC1 (explaining 61% of the gene expression variance) separated the plant genotypes, whereas PC2 (explaining 21% of the gene expression variance) separated the growth conditions (Figure 4a). The PCA also showed that, under control conditions, the WT and *frd3* mutant had highly diverging gene expression phenotypes in roots, whereas upon exposure to high levels of Zn, both profiles were almost similar. In agreement with these observations, differential gene expression analysis [$\log_2$ fold change of $>1$ or $<-1$; false discovery rate (FDR) $< 0.05$] identified 490 differentially expressed genes (DEGs) between WT and mutant roots under control conditions and only five DEGs under high Zn conditions (Figure 4b and Table S1).

Comparison of gene expression in the *frd3* mutant and WT under control conditions revealed the extent of molecular alteration in the *frd3* mutant roots, which involved several processes beyond metal homeostasis. In fact, gene ontology (GO) enrichment analysis (Figure 4c; Table S2) revealed that a large majority of the 368 genes more highly expressed in *frd3* under control conditions were involved in biotic stress (98 genes) hormonal (59 genes) and oxidative stress (43 genes) responses. Metal homeostasis only ranked fourth, with 37 genes more highly expressed in *frd3*, including 26 Fe, nine Zn and six Mn homeostasis related genes, respectively. Finally, 14 genes were involved in the nitric oxide (NO) response (Figure 4c). In this list of 368 genes, a number of genes involved in cell wall (CW) modifications were also found (Figure 4e; Table S1),

 

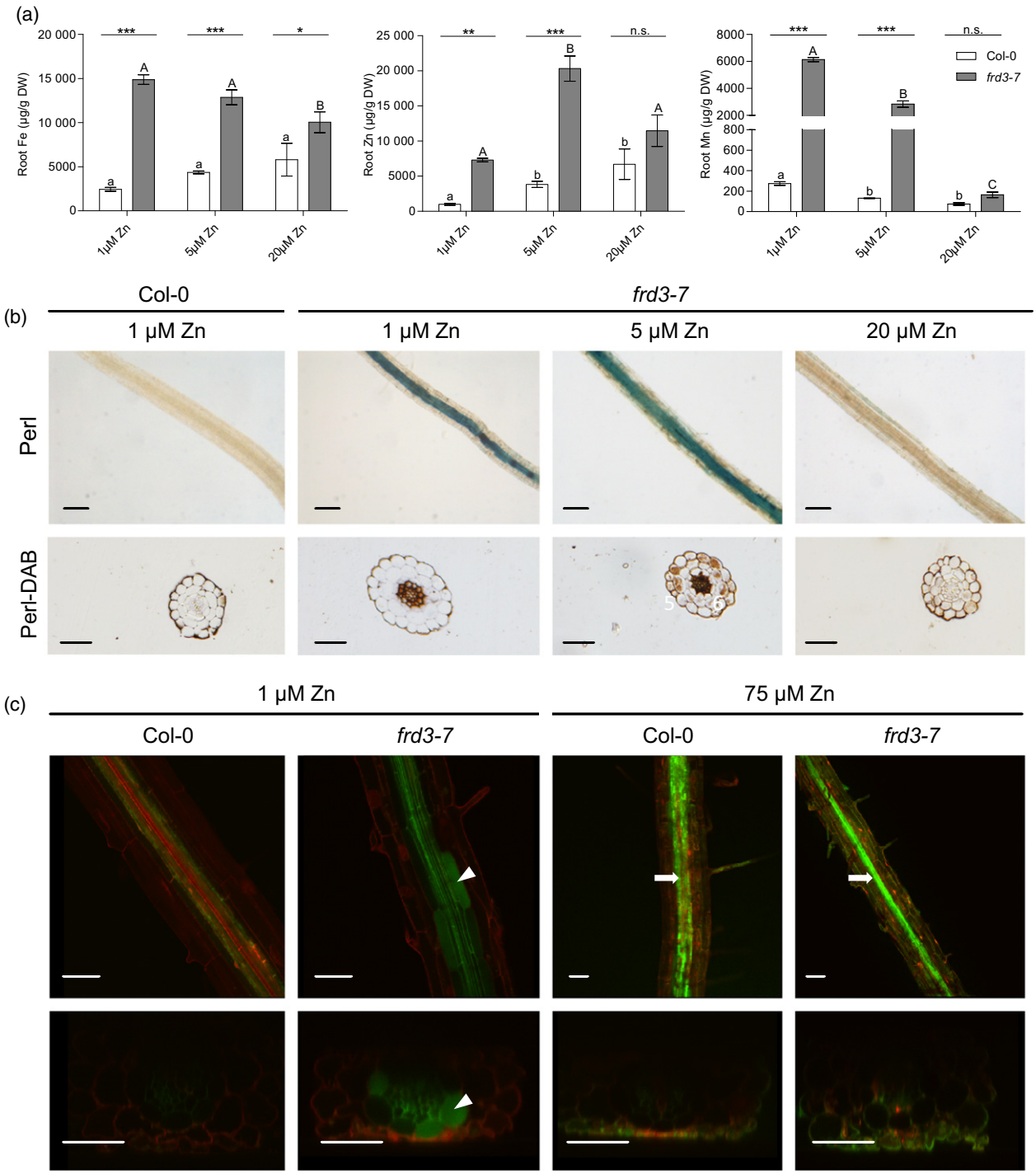


**Figure 2.** Metal accumulation and localization. (a) Fe, Zn and Mn accumulation in roots of Col-0 (white) and *frd3-7* (grey) plants grown in hydropony and exposed to different concentrations of Zn (1, 5 and 20 µM $ZnSO_4$). Data [µg/g dry weight (DW)] represent mean values (± SEMs) of three independent experiments, each including pools of two or three plants per condition and genotype. The data were analyzed by two-way ANOVA and followed by Bonferroni's multiple-comparison post-hoc test. Statistically significant differences between means are indicated by asterisks (within conditions, $*P < 0.05$, $**P < 0.01$, $***P < 0.001$, n.s. not significant) or different letters (within genotypes, $P < 0.05$). (b) Fe visualization by Perl (in blue) and Perl/DAB (in brown) staining in root tissues of Col-0 and *frd3-7* plants grown in hydropony and exposed to different concentrations of Zn (1, 5 and 20 µM $ZnSO_4$). Scale bar: 100 µm (*in toto*) or 50 µm (sections). The pictures are representative of three independent experiments. (c) Zn visualization using the fluorescent probe Zinpyr-1 (green) in roots of Col-0 and *frd3-7* seedlings grown vertically in Petri plates under different Zn conditions (1 and 75 µM $ZnSO_4$). Propidium iodide was used to stain the cell wall (red). Longitudinal and cross optical sections were realized. Arrowheads and arrows show Zn localization in the endodermis and in vasculature cells, respectively. Scale bars: 50 µm. The pictures are representative of three independent experiments. The compared effect of Zn treatment in hydropony or *in vitro* experiments is shown in Figure S4.

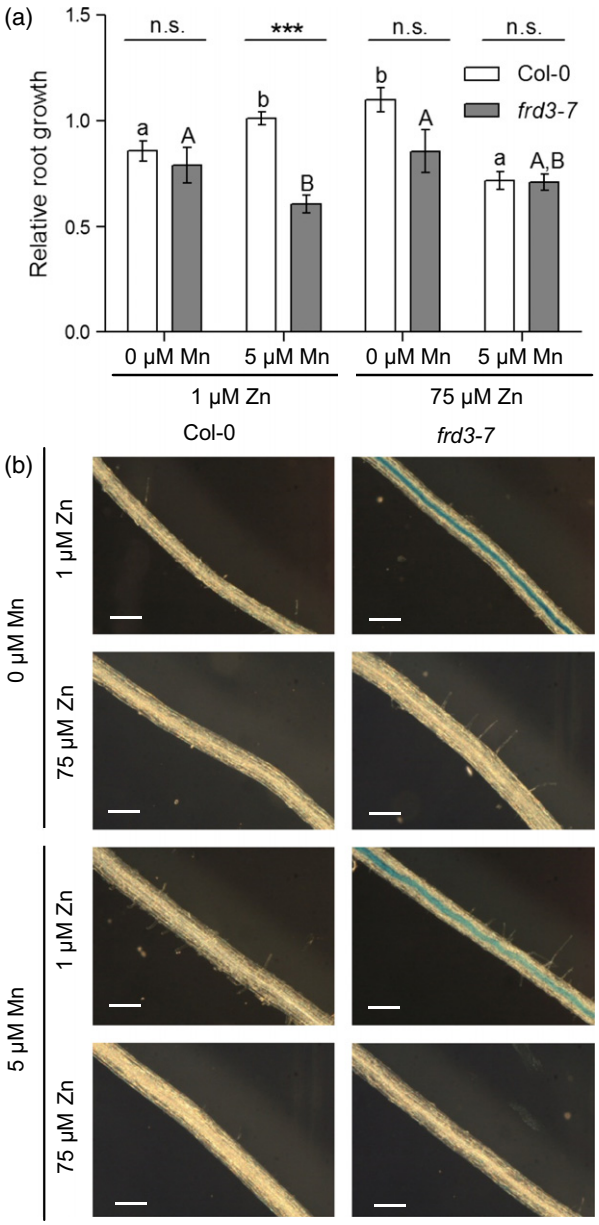


**Figure 3.** Manganese toxicity phenotype. (a) Zn and Mn tolerance assay for Col-0 (white) and *frd3-7* (grey). Seedlings were grown vertically in petri plates under different zinc (1 or 75 µM $ZnSO_4$) and manganese (0 or 5 µM $MnSO_4$) conditions. Root growth is relative to Col-0 at 1 µM $ZnSO_4$ and 5 µM $MnSO_4$. Data are mean values (± SEMs) of two independent experiments, each including three series of seven seedlings per condition and genotype. The data were analyzed by two-way ANOVA followed by Bonferroni's multiple-comparison post-hoc test. Statistically significant differences between means are indicated by asterisks (within conditions, $***P < 0.001$, n.s. not significant) or different letters (within genotypes, $P < 0.05$). (b) Fe accumulation visualized by Perl staining in roots of Col-0 and *frd3-7* seedlings grown vertically in Petri plates in different Zn and Mn conditions, as described above. The pictures are representative of two independent experiments. Scale bars: 100 µm.

including CW restructuring, CW enzymatic activity regulation or lignin biosynthesis. Although no GO enrichment was observed among the 122 genes less expressed in *frd3* compared with the WT under control conditions, this set included a number of genes of interest, such as *FPN1/IREG1* and again genes involved in cell wall modifications (Figure 4d; Table S1).

Upon Zn treatment, the number of DEGs between the WT and the *frd3* mutant strikingly decreased to five genes (Figure 4a,b). Analysis of genes more highly expressed upon Zn exposure in the *frd3* mutant (139 genes) or the WT (69 genes), compared with the WT under control conditions, revealed a similar GO enrichment pattern, highlighting a convergence of gene expression profiles in the two genotypes under high Zn conditions (Figure 4c). This convergence was achieved by: (i) increased expression of Fe and Zn homeostasis genes in the WT, to reach levels similar to the *frd3* mutant (Figures 4c,d and S7); and (ii) decreased expression in the *frd3* mutant of all or most genes involved in biotic stress, oxidative stress, hormonal response or Mn homeostasis, respectively (Figures 4c,e and S7). The latter group of genes largely correlated with the 72 downregulated genes in the *frd3* mutant upon Zn exposure. Altogether, Zn exposure almost totally abolished the secondary gene expression phenotypes of the *frd3* mutant, but the constitutive expression of the Fe-deficiency response was maintained.

### Overexpression of the Fe uptake strategy I

RNA-Seq data and GO enrichment analysis showed that many genes involved in the Fe-deficiency response were constitutively overexpressed in *frd3* roots in both control and high Zn conditions, whereas these genes were induced by high Zn in the WT (Figure 4c,d; Table S2). These data were confirmed by quantitative reverse transcription polymerase chain reaction (qRT-PCR) for three key genes of the Fe-deficiency response in Arabidopsis: *FIT*, *FRO2* and *IRT1*, with 3-, 26- and 30-fold higher expression in the mutant compared with the WT under control conditions, respectively (Figure 5a–c). Under high Zn conditions, the expression level of the three genes was high in both WT and *frd3*. Acidification of the medium, ferric chelate reductase activity and the accumulation of the IRT1 protein followed the same pattern (Figures 5d,e and S8). Altogether, these data confirmed that the constitutive expression of the Fe-deficiency response in the *frd3* mutant was not reversed by exposure to high levels of Zn.

### Oxidative stress in *frd3* mutant roots

Among DEGs, an enrichment of GO terms related to ROS production (43 upregulated genes) and the NO response (14 upregulated genes) in the comparison of *frd3* and WT under control conditions (Figure 4c,e; Table S2) suggested that the mutant roots experienced oxidative stress. This response was partially reversed by exposure to high levels

 

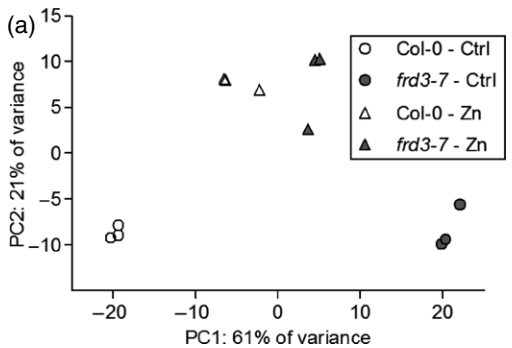


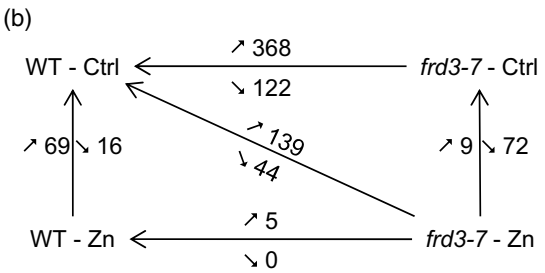


(c)

| GO enriched categories | Up *frd3-7* - Ctrl vs WT - Ctrl | Up *frd3-7* - Zn vs WT - Ctrl | Up WT - Zn vs WT - Ctrl | Down *frd3-7* - Zn vs *frd3-7* - Ctrl |
|---|---|---|---|---|
| Metal: | 37 | 27 | 22 | 7 |
| Zn | 9 | 8 | 6 | 0 |
| Fe | 26 | 20 | 17 | 7 |
| Mn | 6 | 0 | 0 | 0 |
| Oxidative stress | 43 | 14 | 10 | 14 |
| NO | 14 | 8 | 8 | 0 |
| Biotic response | 98 | 0 | 0 | 26 |
| Hormonal response | 59 | 0 | 8 | 17 |
| Total nb of DEGs | 368 | 139 | 69 | 72 |

Nb of regulated genes : 0 1-10 11-20 21-50 50<

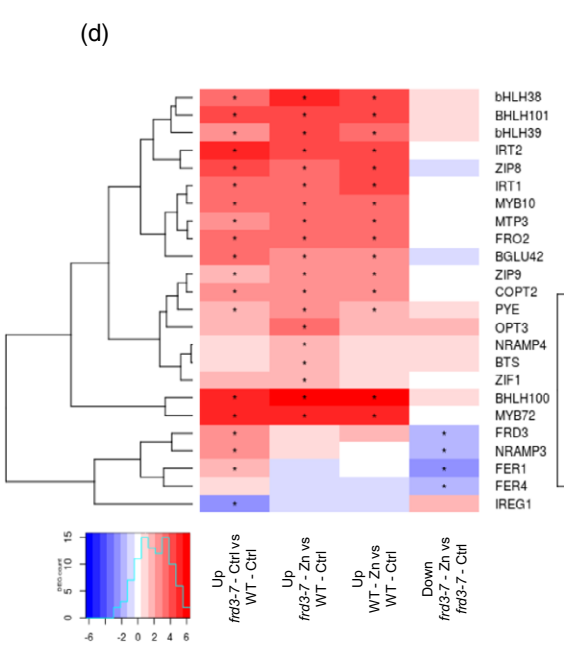


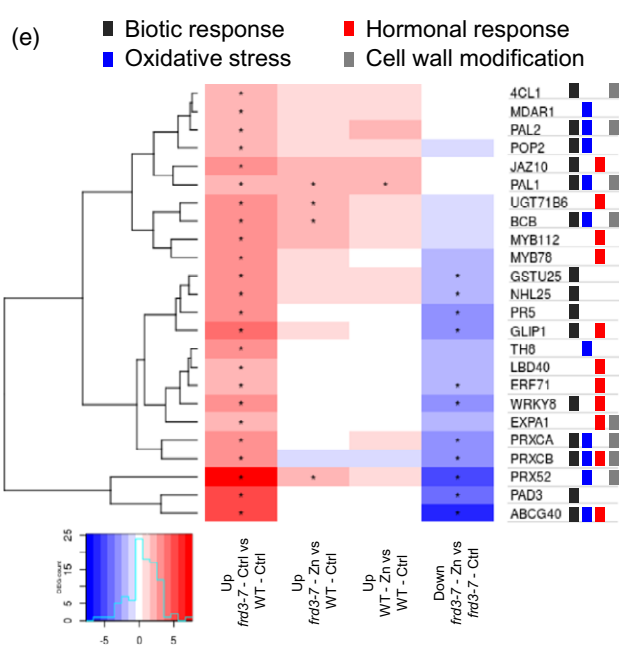

**Figure 4.** Transcriptomic analysis in roots. Col-0 and *frd3-7* plants grown in hydropony and exposed to 1 and 20 μM $ZnSO_4$. RNA-Seq was conducted on RNA from root tissues of three independent experiments each including pools of two or three plants per condition and genotype. (a) Principal component analysis of RNA-Seq gene expression data of Col-0 (white) and *frd3-7* (grey) exposed to 1 μM $ZnSO_4$ (dots) or 20 μM $ZnSO_4$ (triangles). (b) Summary statistics of up- (↗) or down-expressed (↘) genes in different pair-wise comparisons. The arrows indicate the direction of the comparison. (c) Gene ontology (GO) enrichment analysis for selected comparisons. The color code in blue or red indicates the number of down- or up-expressed genes, respectively, within enriched functional categories. (d, e) Heat maps depicting the expression profiles of selected genes involved in metal homeostasis (d) or in biotic (black) and oxidative (blue) stress, hormonal response (red) and cell wall modification (grey) (e) in roots for selected comparisons. Asterisks indicate statistically different expression levels. In (e), colored bars beside gene names correspond to the GO annotation. In (c–e), only comparisons in which a GO enrichment was detected are shown. A heat map including all regulated genes is shown in Figure S7. Gene expression data and GO enrichment results are shown in Tables S1 and S2, respectively.

of Zn in the mutant, with only 14 and eight upregulated genes for ROS production and NO response in mutants exposed to high levels of Zn (Figure 4c, *frd3*-Zn/WT-ctrl comparison). In agreement, $H_2O_2$ accumulation was observed in the root vascular tissues, but not in the WT, under control conditions (Figure S9a), and was suppressed by exposure to high levels of Zn, but not by Mn deficiency (Figure S9a,b). The accumulations of Fe (Figures 2, 3) and $H_2O_2$ (Figure S9) in *frd3* root vascular tissues were thus correlated, suggesting that Fe accumulation was responsible for oxidative stress. Coherently, no $H_2O_2$ accumulation (and no Fe accumulation) was observed in *frd3* roots upon Fe deficiency (Figures S5, S9c).

### Cell wall analysis by Fourier-transform infrared spectroscopy (FTIR)

The RNA-Seq data analysis also showed that a number of genes encoding proteins involved in CW modifications were differentially expressed in the *frd3* mutant compared with the WT under control conditions. Those genes

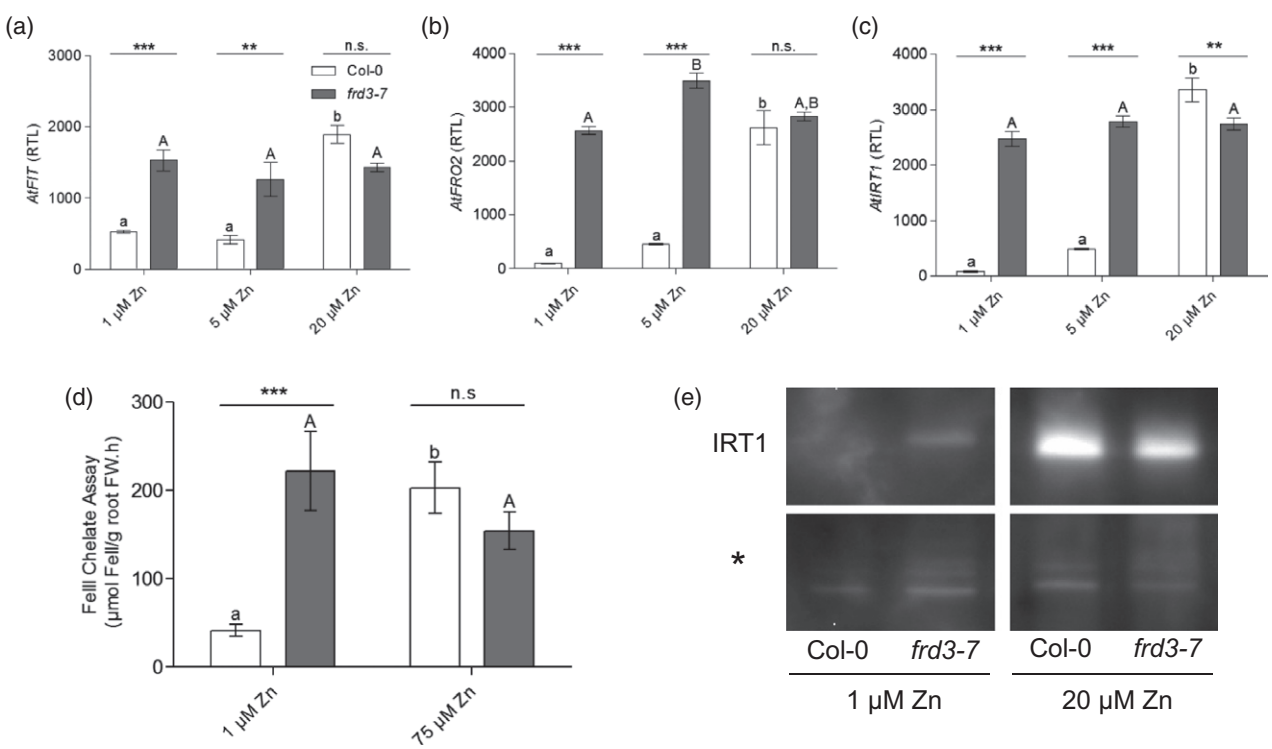


**Figure 5.** Fe uptake strategy. (a–c) Quantitative RT-PCR analysis of the expression of the *AtFIT* (a), *AtFRO2* (b) and *AtIRT1* (c) genes in roots of Col-0 (white) and *frd3-7* (grey) plants grown in hydropony and exposed to different concentrations of Zn (1, 5 and 20 μM $ZnSO_4$). Data (relative transcript level, RTL) represent mean values (± SEMs) of three independent experiments, each including pools of two or three plants per condition and genotype, each analyzed in three technical replicates. (d) FeIII chelate reductase activity in roots of Col-0 (white) and *frd3-7* (grey) seedlings grown vertically in Petri plates under different zinc conditions (1 and 75 μM $ZnSO_4$). Data represent mean values (±SEMs) of two independent experiments, each including between three and six pools of five plants per condition and genotype. (e) IRT1 protein accumulation in roots of Col-0 and *frd3-7* plants grown in hydropony and exposed to 1 and 20 μM $ZnSO_4$. The nonspecific band indicated with an asterisk (*) served as a loading control. The blot is representative of three independent experiments, each including pools of two plants per condition and genotype, each analyzed in two technical replicates. (a–d) The data were analyzed by two-way ANOVA and followed by Bonferroni's multiple-comparison post-hoc test. Statistically significant differences between means are indicated by asterisks (within conditions, $^{**}P < 0.01$, $^{***}P < 0.001$, n.s. not significant) or different letters (within genotypes, $P < 0.05$).

 

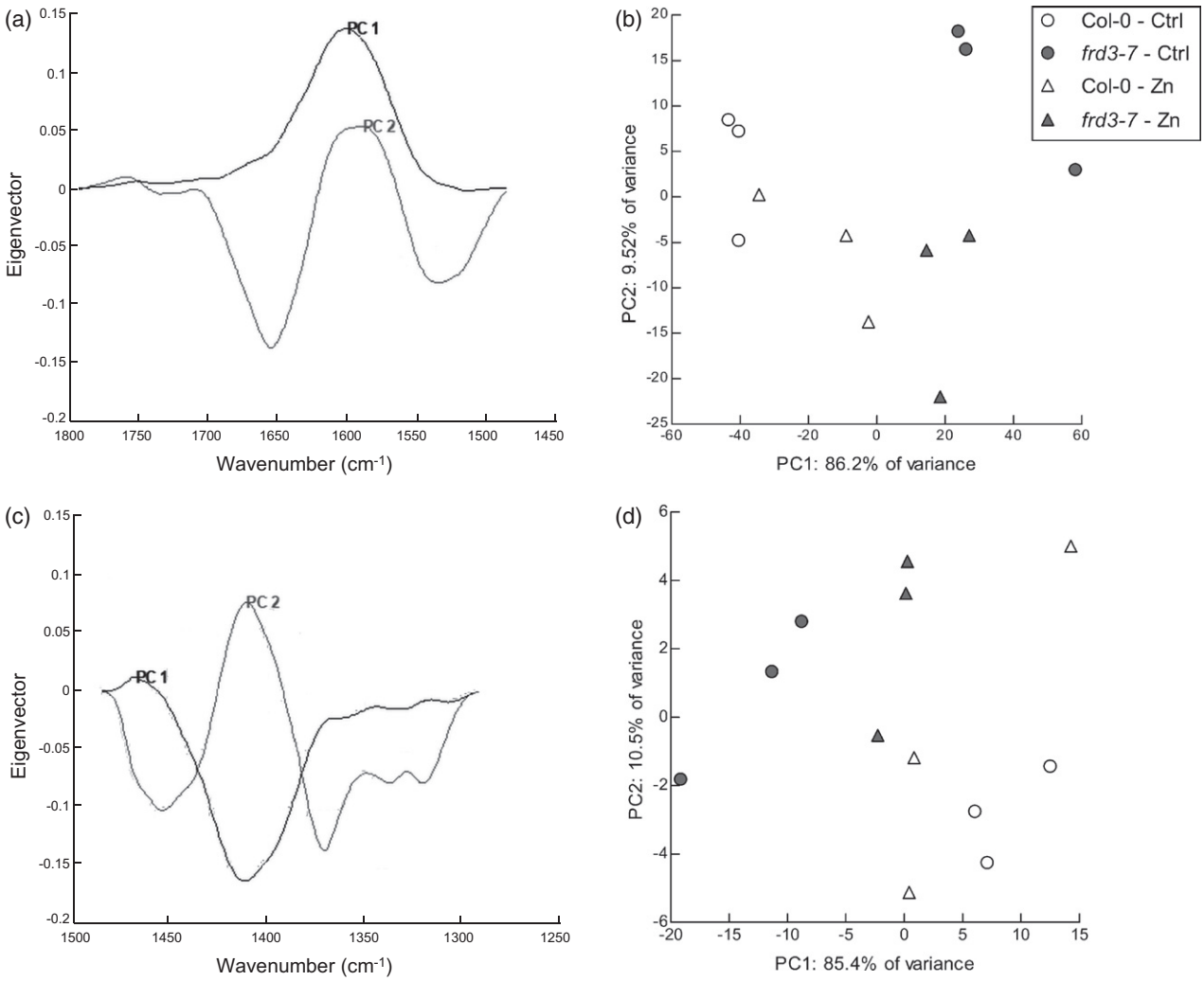


**Figure 6.** Fourier-transform infrared spectroscopy (FTIR) analysis of cell wall in roots of Col-0 and *frd3-7* plants grown in hydropony and exposed to different concentrations of Zn (1 and 20 μM $ZnSO_4$). (a, c) Loading-factor plots for PC1 (principal component 1; dark grey) and PC2 (principal component 2; light grey) explaining principal component analysis (PCA) clustering for wavenumber between (a) 1800–1475 $cm^{-1}$ and (c) 1475–1375 $cm^{-1}$. (b, d) PCA analysis of the FTIR spectra of Col-0 (white) and *frd3*-7 (grey) exposed to 1 μM $ZnSO_4$ (dots) or 20 μM $ZnSO_4$ (triangles). Each dot is the projection of one spectrum on the first and second PCs for wavenumber between (b) 1800–1475 $cm^{-1}$ and (d) 1475–1375 $cm^{-1}$. The spectra were measured from three biological replicates, each including a pool of roots from at least six plants per genotype and treatment.

were downregulated or not influenced by high levels of Zn in the mutant (Figure 4e; Tables S1 and S2). To further examine this response, the CW composition in root tissues of WT and *frd3* plants exposed to control and high Zn conditions was analyzed by FTIR spectroscopy. The spectra were then submitted to a PCA (Figures 6 and S10).

For the 1800–1500 $cm^{-1}$ and 1500 and 1300 $cm^{-1}$ regions of the FTIR spectrum (Figure 6a,b), the PC1s (86.2 and 85.4% of the total variance, respectively) separated the samples according to the genotype and to a lower extent the conditions (Figure 6b,d), and were associated with positive (1600 $cm^{-1}$) and negative (1420 $cm^{-1}$) peaks, corresponding to $COO^-$ antisymmetric and symmetric stretching, respectively (Sene *et al.*, 1994; Jones *et al.*, 2005), which correlate with unesterified pectins (Jones *et al.*, 2005; Alonso-Simón *et al.*, 2011; Meyer *et al.*, 2015). These observations were indicative of a modification of CW structure in the *frd3* mutant under control conditions, corresponding to a lower degree of pectin methylesterification compared with the WT. This is in agreement with the lower expression of a pectin methylesterase inhibitor gene (At5g62360) in the mutant compared with the WT under control conditions (Table S1). Upon exposure to high levels of Zn, the differences in methylesterification of pectins in the mutant and the WT were attenuated (Figure 6b,d).

Moreover, for the 1800–1500 $cm^{-1}$ region of the FTIR spectrum (Figure 6a,b), PC2 (9.52% of the variance) separated the two conditions and can be connected to amide I and amide II [the C=O vibration (1650 $cm^{-1}$) and the N–H vibration (1510–1580 $cm^{-1}$), respectively] with the described intensity ratio of 2/1 (Goormaghtigh *et al.*, 1994; Sene *et al.*, 1994) (Figure 6a and 6b), which correlate with proteins (Alonso-Simón *et al.*, 2011). For the 1500–1300 $cm^{-1}$ region of the FTIR spectrum, the PC2 did not clearly separate the samples (Figure 6d). Finally, for the 1300–900 $cm^{-1}$ region of the FTIR spectrum (associated with polysaccharides; Kačuráková *et al.*, 2000), there were no clear differences between the WT and the mutant (Figure S10).

### Metabolite analysis

As the *frd3* mutant phenotype is characterized by altered Fe mobility, which is at least partially reversed upon exposure to high levels of Zn, the levels of organic acid (e.g. citrate and malate) and nicotianamine (NA) were determined using mass spectrometry in root tissues of WT and *frd3* seedlings exposed to control and high Zn conditions. These metabolites are metal chelators and are involved in metal mobility and sequestration within the plant (Stephan and Scholz, 1993; von Wirén *et al.*, 1999; Haydon and Cobbett, 2007).

Under control conditions, the *frd3* mutant accumulated more citrate (2.6-fold), malate (1.6-fold) and NA (7.5-fold) in the roots compared with the WT (Figure 7). Upon exposure to high levels of Zn, citrate and malate levels remained stable in the mutant but increased to reach similar or higher levels in the WT, respectively (Figure 7a,b). In contrast, NA levels were low and stable in the WT and sharply decreased in the mutant exposed to high levels of Zn (Figure 7c). This observation correlated with the root transcript levels of *NICOTIANAMINE SYNTHASE 2* (*NAS2*), encoding one of the major forms of NA synthase in roots (Klatte *et al.*, 2009): *NAS2* was highly expressed in *frd3* compared with the WT under control conditions, and upon exposure to high levels of Zn was strongly downregulated in the mutant to low levels similar to the levels found in the WT (Figure S11).

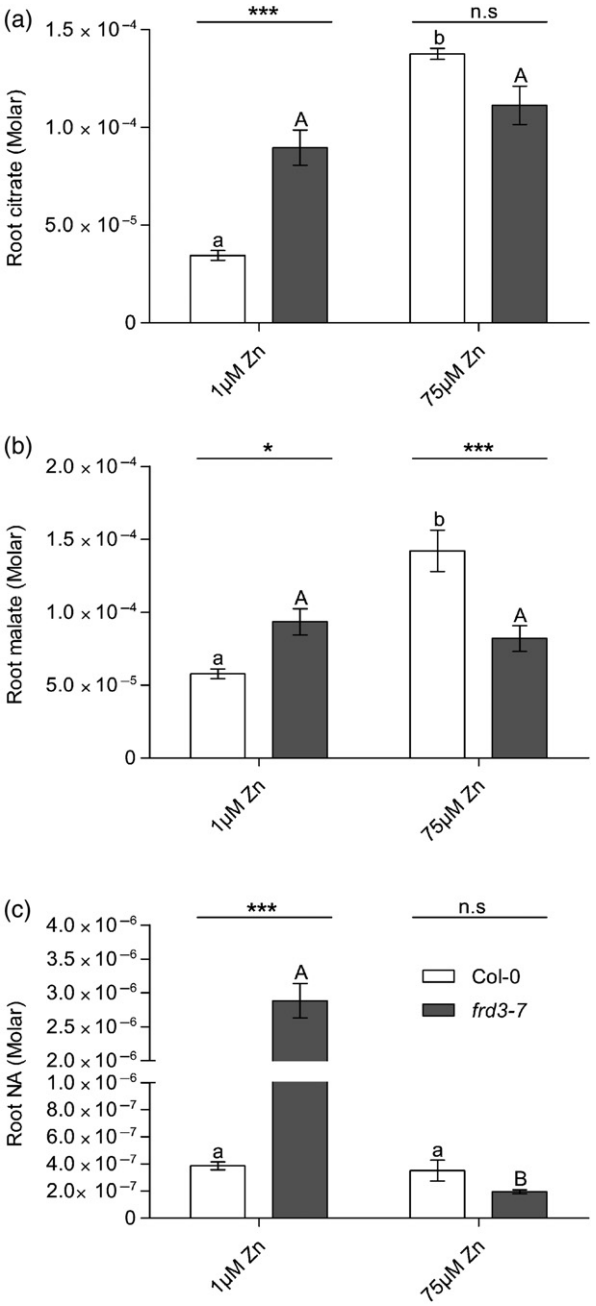


**Figure 7.** Root metal chelator concentration. (a) Citrate, (b) malate and (c) nicotianamine (NA) accumulation in Col-0 (white) and *frd3-7* (grey) seedlings grown vertically in Petri plates under different zinc conditions (1 and 75 μM $ZnSO_4$). Data represent mean values (± SEM) of three independent experiments, each including pools of at least 48 seedlings per condition and genotype, each analyzed in three technical replicates. The data were analyzed by two-way ANOVA followed by Bonferroni's multiple-comparison post-hoc test. Statistically significant differences between means are indicated by asterisks (within conditions, $*P < 0.05$, $***P < 0.001$, n.s. not significant) or different letters (within genotypes, $P < 0.05$).

## DISCUSSION

The phenotype of the *frd3* mutant in Arabidopsis has been described extensively, as a small and chlorotic plant that accumulates Mn, Fe and Zn in tissues, and overexpresses the Fe uptake machinery (Delhaize, 1996; Rogers and Guerinot, 2002; Green and Rogers, 2004; Durrett *et al.*, 2007). It has been attributed to a defect in citrate transport into the xylem in roots and, as a consequence, to the inability of the mutant to translocate Fe to shoot tissues, which are starved of Fe. This phenotype can be rescued by Fe supplementation in the medium. Here, we showed that the *frd3* mutant phenotype not only results from Fe deficiency, but also from multiple consequences of Fe immobilization in the roots. Our data also highlighted the tight

 

interconnection between Fe, Zn, Mn homeostasis, oxidative stress and biotic stress responses (Figure 8a).

**Biotic stress signaling and Fe accumulation in the cell wall**

We showed that Fe accumulation in root vascular tissues, typical of the *frd3* mutant, resulted in $H_2O_2$ accumulation (Figures 8a and S9), which is consistent with the high expression of a large set of oxidative stress genes in *frd3* (Figure 4; Table S2). Fe is highly redox active and is known to induce oxidative stress (Stohs and Bagchi, 1995; Pierre and Fontecave, 1999; Marschner and Marschner, 2012). Our data also suggest that Fe and $H_2O_2$ accumulation in the mutant hitchhikes the biotic stress signaling pathway (Figure 8a), as the biotic stress response is the largest functional category among genes overexpressed in the mutant compared with the WT under control conditions (Figure 4).

(a) *frd3* mutant in control condition (1 μM Zn)

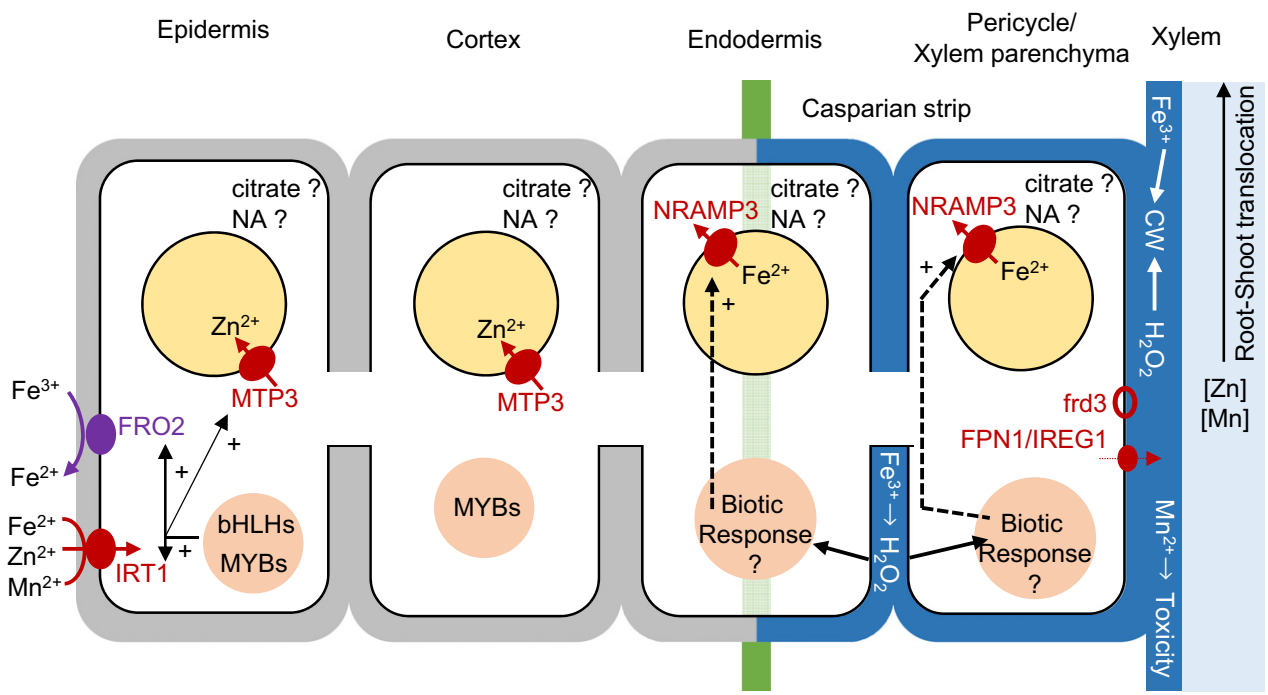


(b) *frd3* mutant in high zinc condition (20 μM Zn)

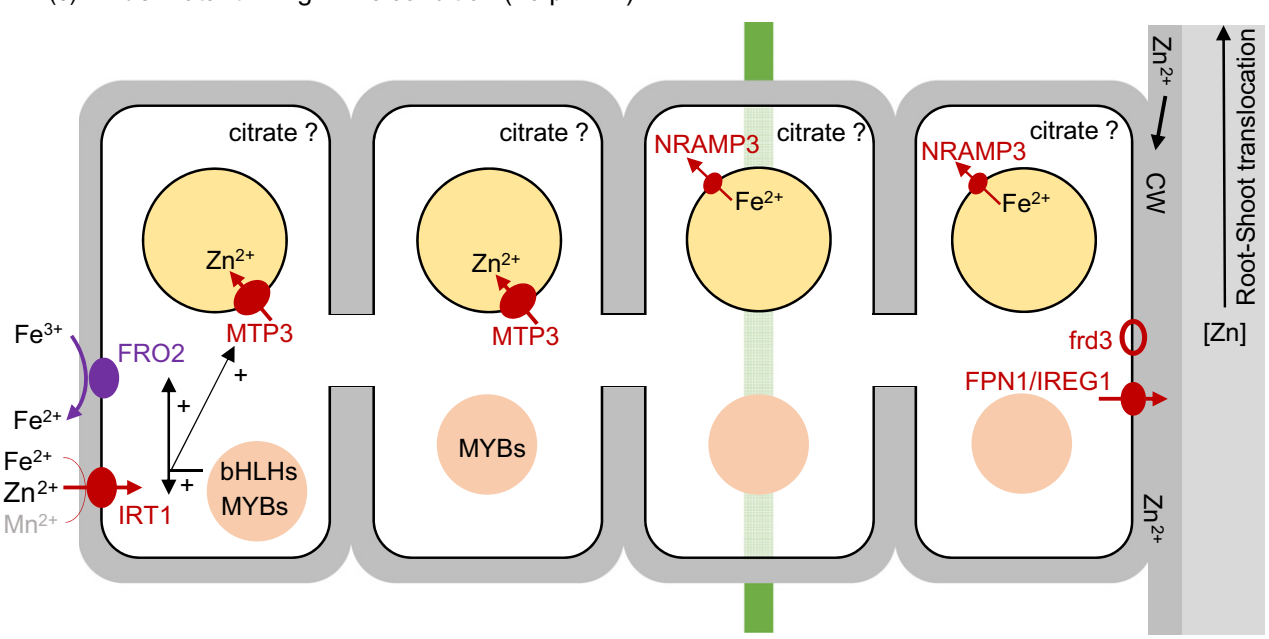

**Figure 8.** A working model representation of the different processes determining the phenotype of an *frd3* mutant plant exposed to (a) control or (b) excess Zn conditions. Note that only the processes that take place differently between the mutant and the WT or that are altered by Zn in the mutant are represented. (a) In control conditions, a shoot-born Fe deficiency signal (not represented) induces a strong Fe-deficiency response in roots, via the action of bHLH and MYB transcription factors, resulting in the strong and constitutive expression of, among others, *FRO2*, *IRT1* and *MTP3* (Figures 4 and 5), in the increased synthesis of citrate as well as NA (Figure 7), and in the increased uptake of Fe, but also of Zn and Mn (Figure 2). Zn and Mn also accumulate in the shoot (Figure S3). $Fe^{3+}$ accumulation in the cell wall (CW) of the endodermis, pericycle and vascular root tissues, as evidenced by Perls staining (Figure 2), is responsible for $H_2O_2$ accumulation (Figure S9). Accumulation of Fe and $H_2O_2$ in the CW modifies its structure (Figure 6) and triggers an oxidative and biotic stress response, including among others the induction of *NRAMP3* (Figure 4). On the other hand, Mn accumulation in the root CW is strongly toxic (Figure 3). (b) Upon exposure to high levels of Zn, Zn competes with Fe for binding to the CW, resulting in reduced Fe binding to the CW (Figure 2), in a reduction of the oxidative burden, and in the downregulation of the biotic stress response (Figures 4 and S9). Fe remains inaccessible for shoots and the Fe-deficiency response is fully maintained, however, including citrate synthesis (Figures 4, 5 and 7). In contrast, NA accumulation in root tissues is strongly reduced (Figures 7 and S11). Zn also competes with Mn uptake, and almost completely abolishes root and shoot Mn accumulation (Figures 2 and S3). Reduced Mn accumulation and oxidative burden at high Zn levels partially restore root growth in the *frd3* mutant (Figure 1). Key: yellow circles, vacuoles; orange circles, nuclei; green, casparian strip; blue: $Fe^{3+}$ accumulation, as evidenced by Perls staining; ?, processes for which the precise tissular location is not known. The tissue-specific expression of different genes is represented based on data from original articles cited in the Introduction and the Discussion: bHLH, basic helix-loop-helix; CW, cell wall; FRD3, Ferric Reductase Defective 3; FPN1/IREG1, Ferroportin 1/Iron REGulated 1; FRO2, Ferric Reductase-Oxidase 2; IRT1, Iron-Regulated Transporter 1; MTP3, Metal Tolerance Protein 3; MYB, myeloblastosis; NA, nicotianamine; NRAMP3, Natural Resistance-Associated Macrophage Protein 3. The size of the bubbles representing membrane transporters is representative of their expression level, based on transcript or protein levels. The model is further detailed and contextualized in the Discussion.

As a matter of fact, both Fe and $H_2O_2$ accumulation have been linked to pathogen response. Upon pathogen attack, the role of ROS, including $H_2O_2$, as signals for the induction of defense genes and as a weapon for pathogen elimination is well documented (Levine *et al.*, 1994; Torres *et al.*, 2006; Piterková *et al.*, 2013; Aznar *et al.*, 2014; Kadota *et al.*, 2015; Suzuki and Katano, 2018). In addition, several genes involved in Fe or other metal homeostasis, which are highly expressed in the *frd3* mutant (Figure 4d), directly contribute (e.g. *MYB72* and *BGLU42*) (Palmer *et al.*, 2013; Zamioudis *et al.*, 2014; Zamioudis *et al.*, 2015) or have been linked (e.g. *NRAMP3*, *NRAMP4* and *YSL3*) (Segond *et al.*, 2009; Chen *et al.*, 2014) to pathogen resistance or plant–microbe beneficial interactions (Verbon *et al.*, 2017; Romera *et al.*, 2019). Several studies have also suggested that the Fe status of the plant influences pathogen virulence (Kieu *et al.*, 2012; Koen *et al.*, 2014). Moreover, it was shown in wheat that a pathogen attack induces a cellular remobilization and accumulation of Fe in the leaf apoplast, causing local Fe deficiency in the cytosol and the production of ROS, resulting in an oxidative burst in the apoplast. Those events trigger the transcriptional activation of pathogen response genes (Liu *et al.*, 2007). As suggested for NA (Schuler *et al.*, 2011), it thus appears that the defect in citrate transport from the pericycle in the *frd3* mutant, and the resulting Fe-deficiency response and accumulation of Fe in the root cell walls, mimics the initial steps of a biotic stress response (Figure 8a), which possibly contributes to the dwarfed phenotype of the mutant.

### Fe and citrate xylem loading coordination

The ferroportin FPN1/IREG1 is suggested to act in Fe loading into the xylem (Morrissey *et al.*, 2009). The downregulation of the *FPN1/IREG1* gene in the roots of the *frd3* mutant compared with the WT is interesting to note (Figure 4d; Table S1). It suggests that Fe translocation to the shoot may be repressed in the *frd3* mutant, and that citrate and Fe transport, by FRD3 and FPN1/IREG1, respectively, may be coordinated. How such coordination is achieved is unclear. Indeed, in contrast to *FPN2* (Schaaf *et al.*, 2006; Morrissey *et al.*, 2009), *FPN1* and *FRD3* are not part of the FIT regulon (Colangelo and Guerinot, 2004; Mai *et al.*, 2016) and are therefore not co-regulated with *IRT1*, *FRO2* and others in response to Fe deficiency (Figures 4d and 6). Furthermore, *FRD3* expression, but not *FPN1* expression, is altered in the *pye* mutant (Long *et al.*, 2010).

### The super toxic Mn

The strong activation of the Fe uptake system in the *frd3* mutant also results in massive Mn accumulation (Delhaize, 1996), essentially in CW (Green and Rogers, 2004), and Mn toxicity (Figures 2, 3, 8a). Mn is in fact the second most phytotoxic metal (Millaleo *et al.*, 2013), and an excess of Mn was shown to cause growth reduction (Lei *et al.*, 2007; Millaleo *et al.*, 2013), for instance. In the *frd3* mutant, Mn toxicity did not result from $H_2O_2$ accumulation (Figure S9) (Demirevska-Kepova *et al.*, 2004; Lei *et al.*, 2007).

### CW modification and metal binding

Both FTIR and RNA-Seq data suggest that the CW structure is modified in the *frd3* mutant, possibly resulting in a lower degree of pectin methylesterification (Figure 6). The CW acts as a barrier, preventing the entry of metals into plant cells, and as an extracellular storage compartment, limiting the toxic effects of excess metals (Krzesłowska, 2011). The degree of pectin methylesterification is important for metal tolerance. Indeed, pectins with a low degree of methylation are rich in free carboxyl groups that can bind di- and trivalent metals. A low degree of pectin methylation has been associated with Fe accumulation in the CW (Ye *et al.*, 2015).

Moreover, high expression of CW biosynthesis genes (e.g. *EXPA1*, *4CL1*, *PRXCA* and *PRXCB*, and *PAL1* and *PAL2*; Figure 4e; Tables S1 and S2) was also observed in the mutant (Figure 8a). Several of these genes belong to the phenylpropanoid pathway, which is important for the production of many secondary plant metabolites (e.g. flavonoids), but is also important for lignin biosynthesis (Le Gall *et al.*, 2015). Metal stress is known to increase lignin biosynthesis (Moura *et al.*, 2010). For instance, lignin biosynthesis is induced during copper (Cu) stress (Ali *et al.*, 2006; Lequeux *et al.*, 2010) or aluminum (Al) exposure (Chandran *et al.*, 2008). Furthermore, the level of ROS (mostly $H_2O_2$) and cell wall peroxidases are important for lignin polymerization and the cross-linking of proteins and polysaccharides in the CW (Ranieri *et al.*, 2003).

**Zn to the rescue**

Exposure to high levels of Zn had a strong impact on the *frd3* mutant, with unexpectedly improved root growth compared with plants grown in control conditions (Figure 1). Zn reduced or abolished many phenotypes observed in the mutant (Figure 8b): Mn accumulation and toxicity, ROS and Fe accumulation in the vascular tissues, biotic stress response and CW modifications. As highlighted by the PCA of both RNA-Seq and FTIR data (Figures 4a and 6b,d), the molecular phenotypes of the WT and the *frd3* mutant largely converged with exposure to high levels of Zn.

The one phenotype that Zn did not alleviate was the constitutive expression of the Fe uptake mechanisms, a trait shared by both WT and mutant plants in the presence of high levels of Zn (Figures 4 and 5). It is well documented that Zn excess causes Fe deficiency in Arabidopsis (Fukao *et al.*, 2011; Shanmugam *et al.*, 2011; Pineau *et al.*, 2012; Shanmugam *et al.*, 2012; Mendoza-Cózatl *et al.*, 2014). In the *frd3* mutant, high expression of the Fe uptake system might be triggered by a similar response or by a shoot-born Fe deficiency signal or both (Figures 4, 5, 7, 8b and S7).

The reversal of the other *frd3* phenotypes by high levels of Zn possibly results from competition between Zn, Fe and Mn for transport and/or binding (Figure 8b). Indeed, according to the Irving Williams series (Pd > Cu > Ni > Co > Zn > Cd > Fe > Mn > Mg), each metal presents a different affinity for potential binding sites and therefore metal replacements can occur (Irving and Williams, 1953; Krämer *et al.*, 2007). For instance, in the presence of equimolar concentrations of Zn, Cu and Fe, both Cu and Zn are coupled to ligands, to the detriment of Fe (Gayomba *et al.*, 2015). It is has also been known for a long time that the CW is a major actor for Zn tolerance by governing the cellular pool of free Zn in plants (Turner, 1970; Turner and Marshall, 1972), with the root apoplast being a major Zn storage compartment (Schmid *et al.*, 1965; Jiang and Wang, 2008).

In the *frd3* mutant with exposure to high levels of Zn, we suggest several hypotheses. First, Zn may displace Fe from its binding sites in the CW. As Zn is a non-redox active metal, contrary to Fe (Broadley *et al.*, 2007), its interactions with thiol groups in the CW would prevent oxidative damage, abolishing the oxidative stress response and hence the biotic stress response observed in the mutant under control conditions (Figure 8b). It was shown that the Fe-deficiency response and the induced systemic resistance (ISR) in the presence of beneficial microbes share approximately 20% of differentially expressed genes, suggesting that the Fe-deficiency response is part of the ISR (Zamioudis *et al.*, 2015). As it is abolished by high levels of Zn, the biotic response in the *frd3* mutant clearly results from Fe, and consequently $H_2O_2$ accumulation, in the CW, and is not triggered by Fe deficiency, which persists in the mutant. Moreover, the CW modifications observed in the mutant under high levels of Zn (Figure 6) can also be explained by reduced oxidative burden, which is, among others, important for lignin polymerization (Ranieri *et al.*, 2003), and by the increased methylesterification of pectins triggered by Zn in the CW (Muschitz *et al.*, 2015). Alternatively, Zn may also alter intracellular trafficking of Fe, via its strong effect on NA root content (see below and Figure 7c) (Klatte *et al.*, 2009; Haydon *et al.*, 2012), to limit Fe access to the CW (Figure 8b). It is also possible that Zn acts both in the apoplast and in the cytosol (Figure 8b).

Exposure to high levels of Zn has a dramatic effect on Mn accumulation in the *frd3* mutant (Figures 2 and S3), most likely resulting from competition for uptake between Mn and Zn, possibly via ZIP transporters that are highly expressed in the mutant (Figure 4d; Tables S1 and S2). As Mn accumulation is toxic for the *frd3* mutant (Figure 3), its reduction is certainly contributing to improved growth of the mutant at high levels of Zn (Figure 8b).

Finally, as part of the Fe-deficiency response (Brouquisse *et al.*, 1986; de Vos *et al.*, 1986; Abadía *et al.*, 2002; Rogers and Guerinot, 2002; Li *et al.*, 2008), citrate, malate and NA accumulated in the roots of the *frd3* mutant under control conditions (Figures 7 and 8a). Citrate accumulation occurred in the mutant, despite a 40% reduction in citrate level in the xylem sap (Rogers and Guerinot, 2002). NA accumulation correlated with high expression of *NAS2* (Figure S11), which is known to be induced by Fe deficiency in roots (Klatte *et al.*, 2009). With high levels of Zn, the organic acid concentrations remained high in the *frd3* mutant and increased in the WT, in agreement with the observed positive correlation between organic acids and Zn tolerance (Godbold *et al.*, 1983, 1984), and with their accumulation under conditions of Fe deficiency (Brouquisse *et al.*, 1986; de Vos *et al.*, 1986; Abadía *et al.*, 2002; Li *et al.*, 2008). In contrast, NA levels and *NAS2* expression (Figures 7c and S11) were strongly reduced in the *frd3* mutant upon exposure to high levels of Zn, suggesting that

a hierarchy exists between the activating and repressive effects of Fe (Klatte *et al.*, 2009) and Zn (Talke *et al.*, 2006) on *NAS2* expression, respectively (Figure 8b).

### Conclusion

We reported here that the *frd3* mutant phenotype results from mechanisms more complex than Fe mislocalization and deficiency. Indeed, we showed that Mn toxicity significantly contributes to the root growth defect in the mutant, and that Fe mislocalization in CW triggers a biotic stress response through ROS production. We also showed that Zn, by effectively competing with Fe in the CW, can interfere with these mechanisms and restore root growth in the mutant. Altogether, our data shed light on the interactions that exist between Fe, Zn and Mn homeostasis and the oxidative and biotic stress responses, and the key role of the CW in these processes.

## EXPERIMENTAL PROCEDURES

### Plant material and growth conditions

All experiments were conducted with *Arabidopsis thaliana* (Col-0) as the wild type and the Arabidopsis *frd3-7* mutant (in the Col-0 background) (Roschzttardtz *et al.*, 2011). Seeds were surface-sterilized and germinated on half-strength MS medium (Duchefa Biochimie, https://www.duchefa-biochemie.com) supplemented with sucrose (1% w/v; Duchefa Biochimie) and agar (0.8% w/v Select Agar; Sigma-Aldrich, https://www.sigmaaldrich.com). For hydroponics experiments, the seedlings were transferred 2 weeks after germination in hydroponic trays (Araponics, http://www.araponics.com), grown for 3 weeks in control Hoagland medium, then submitted to experimental conditions for an additional 3 weeks. The nutrient solution was exchanged with fresh medium once a week and for the last 3 days before harvest. For plate experiments, seedlings were transferred 5 days after germination on solid Hoagland (0.8% w/v Select Agar in square plastic Petri plates; Greiner Bio-One, https://www.gbo.com). The control Hoagland medium was modified as described by Talke *et al.* (2006) and Hanikenne *et al.* (2008), and included 1 μM Zn ($ZnSO_4.H_2O$), 5 μM Mn ($MnSO_4.H_2O$) and 10 μM FeIII-HBED [*N*,*N*-di-(2-hydroxybenzyl) ethylenediamine *N*,*N*-diacetic acid monohydrochloride]. Zn, Mn and/or Fe were omitted from the medium for deficiency experiments and were added as indicated for excess experiments. All experiments were realized under 8 h light (100 μM photon $m^{-2}$ $s^{-1}$, 22°C)/16 h dark (20°C) in a climate-controlled growth chamber. Unless otherwise stated, all experiments were conducted three times independently. Details on experimental replication are provided in the figure legends.

### Chlorophyll content

Two or three leaves per plant were weighed, then incubated in the dark for 40 h in ethanol (95%, VWR). Discolored leaves were removed and the solution was then analyzed using a spectrophotometer (Genesys20; ThermoFisher Scientific, https://www.thermofisher.com), measuring absorbance at 649 and 665 nm. Total levels of chlorophyll were calculated using the equation: chl *a* + chl *b* = [6.1*(A665) + 20.4*(A649)]/fresh weight (in mg) (Wintermans and De Mots, 1965; Lichtenthaler and Buschmann, 2001).

### Analysis of metal contents

Root and shoot tissues were harvested separately. Root tissues were desorbed and washed as described by Talke *et al.* (2006), and shoot tissues were rinsed in distilled water. After drying at 60°C for 3 days, 10–30 mg of tissue was digested on a DigiPrep Graphite Block Digestion System (SCP Science, http://www.scpscience.com) with 3 mL $HNO_3$ (≥ 65% v/v; Sigma-Aldrich) in DigiPrep tubes. The digestion program was: 15 min at 45°C, 15 min at 65°C and 90 min at 105°C. After digestion, volumes were adjusted to 10 mL with distilled water and 200 μL of $HNO_3$ (≥65% v/v; Sigma-Aldrich). Element concentrations were determined by inductively coupled plasma-atomic emission spectroscopy (Vista AX; Varian).

### Fe and hydrogen peroxide staining

For Fe Perls staining, root samples were vacuum infiltrated with HCl (4% v/v) and K-ferrocyanide (II) (4% w/v; Sigma-Aldrich) at equal volume (1/1) for 10 min and incubated for 30 min at room temperature (20–22°C). The reaction was stopped by substituting the solution with distilled water (Roschzttardtz *et al.*, 2009, 2011). Images were taken using a binocular (SMZ1500; Nikon, https://www.nikon.com) equipped with a camera (Digital Sight DS-5M; Nikon). For In Situ Perls/DAB/$H_2O_2$ intensification, root tissues were vacuum infiltrated with paraformaldehyde (2% w/v), glutaraldehyde (1% v/v) and caffeine (1% w/v) in phosphate buffer (0.1 M; pH 7) for 30 min and incubated overnight in the solution (Roschzttardtz *et al.*, 2009, 2011). The tissues were then washed three times in phosphate buffer (0.1 M, pH 7.4) and dehydrated in successive baths for 2 h each [50, 70, 90, 95 and 100% ethanol, butanol/ethanol (1/1) and 100% butanol]. Technovit 7100 resin (Kulzer, https://www.kulzer.com) was used to embed tissues and 3 μm sections were realized and deposited on glass slides. The slides were then incubated for 45 min in Perls staining solution (as described above), followed by DAB intensification as described previously (Roschzttardtz *et al.*, 2009, 2011). Observation was realized using a binocular (AZ100; Nikon) equipped with a camera (Digital Sight DS-Ri1; Nikon).

Detection of $H_2O_2$ in root tissues was carried out according to the protocol described by Baliardini *et al.* (2015). Briefly, root samples were vacuum infiltrated for 15 min with 3-3-diaminobenzidine tetrahydrochloride (1.25 mg/mL; DAB; Sigma-Aldrich), Tween-20 (0.05% v/v) and $Na_2HPO_4$ (200 mM) and incubated for 45 min in the same solution. Then the roots were bleached in acetic acid/glycerol/ethanol (1/1/3) for 5 min at 100°C, and then stored in glycerol/ethanol (1/4) before observation. Observation was performed using a binocular (SMZ1500; Nikon) equipped with a camera (Digital Sight DS-5M; Nikon).

### Zinc imaging

Root tissues were washed three times for 5 min in distilled water then for 5 min in EDTA (10 mM) to remove metal ions attached to the root surface. Plants were transferred in Zinpyr-1 (10 μM, in water, Sigma-Aldrich) for 2 h in the dark then washed in distilled water (Sinclair *et al.*, 2007; Hanikenne *et al.*, 2008). To visualize the root cell wall, tissues were bathed in propidium iodide (33 μg/mL) for 1 min. Images were collected using an SP2 confocal microscope (Leica, https://en.leica-camera.com), as described by Tillemans *et al.* (2006). Zinpyr-1 was visualized using an argon ion laser ($\lambda_{ex}$ = 488 nm; $\lambda_{em}$ = 500–535 nm) and a helium–neon laser ($\lambda_{ex}$ = 543 nm; $\lambda_{em}$ = 600–730 nm) was used for propidium iodide.

 

### RNA-Seq and qRT-PCR analysis

Upon harvesting, plant root tissues were blotted dry, immediately frozen in liquid nitrogen and stored at −80°C. Total RNAs were prepared using 100 mg of homogenized tissues and RNeasy Plant Mini kit with on-column DNase treatment (Qiagen, https://www.qiagen.com). Libraries for RNA-Seq were prepared from 1 μg of total RNAs with the TruSeq Stranded mRNA Library Prep Kit (Illumina, https://www.illumina.com), multiplexed and sequenced in two runs with an Illumina NextSeq500 device (high-throughput mode, 75 base single-end reads) at the GIGA-R Sequencing platform (University of Liège), yielding on average approximately 22 million reads per sample. Read quality was assessed using FASTQC 0.10.1 (http://www.bioinformatics.babraham.ac.uk/projects/fastqc/). Quality trimming and the removal of adapters were conducted using TRIMMOMATIC 0.32 (Bolger *et al.*, 2014), with the following parameters: trim bases with quality score lower than Q26 in 5 and 3 of reads; remove any reads with $Q < 26$ in any sliding window of 10 bases; crop one base in 3 of all reads; and discard reads shorter than 70 bases. Overall, the quality filtering discarded between 7 and 9% of the raw reads. The Arabidopsis reference genome sequence (TAIR10) and annotation (201606 version) files were downloaded from Araport on 16 September 2016 (https://www.araport.org). Read mapping on the genome was achieved using TOPHAT 2.1.1, with the following parameters: --read-mismatches 2; --min-intron-length 40; --max-intron-length 2000; 2 --report-secondary-alignments; --no-novel-juncs and providing an indexed genome annotation file. Raw read counts were obtained using HTSEQ-COUNT 0.6.1p1, and differentially expressed genes were identified by pairwise comparisons with DESEQ2 1.12.3 (Love *et al.*, 2014). Genes were retained as differentially expressed when the $\log_2$ fold-change (FC) was >1 or <−1, with a Benjamini–Hochberg FDR adjusted *P*-value of <0.05. PCA plots were created with the *PlotPCA* function from R using rlog transformed data (Beginner's guide, DESEQ2 package, 13 May 2014, http://www.bioconductor.org/packages/2.14/bioc/vignettes/DESeq2/inst/doc/beginner.pdf). GO enrichment analyses were conducted using the Thalemine tool on Araport (https://www.araport.org). The heat maps were constructed using the heatmap.2 function of the GPLOTS R package.

For qRT-PCR, cDNAs were synthesized with the RevertAid H Minus First Strand cDNA Synthesis Kit (Fisher Scientific, https://www.fishersci.co.uk) using Oligo(dT) and 1 μg of total RNAs. Quantitative PCR was performed in an ABI Prism 7900HT system (Applied Biosystems, now ThermoFisher Scientific) using 384-well plates and Mesa Green qPCR MasterMix (Eurogentec, https://secure.eurogentec.com), as described by Nouet *et al.* (2015). Primer reaction efficiencies (LINREGPCR 2016.1; Ruijter *et al.*, 2009; Nouet *et al.*, 2015; Table S3) were used to calculate relative gene expression levels by normalization using the *EF1α* and *UBQ10* reference genes and QBASE (https://www.qbaseplus.com/; Hellemans *et al.*, 2007). Their adequacy to normalize gene expression in the experimental conditions was verified using GENORM in QBASE (Vandesompele *et al.*, 2002).

### IRT1 Western blot

Total proteins were extracted from 100 mg of frozen root tissues as described by Séguéla *et al.* (2008). The Western blot was conducted using an IRT1 antibody, as described by Schvartzman *et al.* (2018).

### Acidification and FeIII chelate reductase activity assays

The FeIII chelate reductase activity and acidification assays were conducted as described by Yi and Guerinot (1996). For the acidification assay, seedlings were transferred after 3 days of treatment on Bromocresol media [Bromocresol Purple (0.006% w/v; Carl Roth, https://www.carlroth.com); $CaSO_4$ (0.2 mM); agar (Agar Select 0.8% w/v; Sigma-Aldrich); pH 6.5] for 18 h. For the FeIII chelate reductase activity assays, seedlings were pooled (5 by 5) and roots were immersed in the reductase solution [FeIII-EDTA (0.1mM; Carl Roth); FerroZine (0.3 mM; Acros Organics, https://www.acros.com)] for 20 min in the dark. The absorbance of the FeII–FerroZine complex formed in the solution was measured at 562 nm. The root weight of the sample and the molar extinction coefficient of the complex (28.6 $mM^{-1}$ $cm^{-1}$) were used for the final calculation.

### FTIR analysis

Cell wall (CW) extraction and FTIR analysis from roots and shoots was performed according to the methodology of Zornoza *et al.* (2002) and Meyer *et al.* (2015). Root samples (100 mg dry material) were washed consecutively three times in ethanol (80% v/v), once in chloroform/methanol (2/1 v/v) and three times in acetone. For each washing step, samples were vortexed, agitated (30 min) and centrifuged (1200 ***g***; 5 min) before going to the next step. Final pellets of CW were dried overnight (67°C).

All measurements were performed as described by Meyer *et al.* (2015) with a Bruker Equinox 55 FTIR spectrometer (Bruker, https://www.bruker.com) equipped with a liquid $N_2$ refrigerated mercury cadmium Telluride detector, as described by Goormaghtigh *et al.* (1999) and Meyer *et al.* (2015). To detect CW modification, the FTIR measurements were recorded between 1800 $cm^{-1}$ and 800 $cm^{-1}$. Each spectrum was obtained by averaging 128 scans recorded at a resolution of 2 $cm^{-1}$. FTIR data were analyzed (substraction of water vapor contribution, baseline correction and normalization of the spectra) as described by Meyer *et al.* (2015). To identify differences among populations, PCA was used to reveal spectral contributions that explained most of the variance present in the data set (Johnson and Wichern, 2002).

### Mass spectrometry

Samples were prepared as described by Klatte *et al.* (2009) and Haydon *et al.* (2012). Frozen plant tissues (60 mg) was ground to a fine powder in a tissue grinding mill (1 min, 25 Hz, cold with liquid nitrogen, MM200; Retsch, https://www.retsch.com) and extracted in distilled water at 80°C (500 μL; pre-warmed at 60°C). After a shaking (500 rpm for 15 min), both the extraction step and the shaking were repeated. Cell debris was removed from the samples by two centrifugations (15 000 ***g*** for 20 min). First, a mass spectrometry analysis of standard solutions of malate (1 mg $mL^{-1}$; Sigma-Aldrich), citrate (1 mg $mL^{-1}$; Sigma-Aldrich) and nicotianamine (1 mg $mL^{-1}$; Carbosynth, https://www.carbosynth.com) was performed to determine each *m*/*z* and make a calibration curve. To quantify malate, citrate and nicotianamine, each sample was analyzed using the standard addition method. All measurements were performed on the SYNAPT G2 HDMS spectrometer (Waters, https://www.waters.com) fitted with an electrospray ionization source used in negative mode. The instrument has been described extensively previously (Giles *et al.*, 2004; Pringle *et al.*, 2007; Shvartsburg, 2008; Shvartsburg and Smith, 2008). A weighed standard tartaric acid (Sigma-Aldrich) solution was prepared with Milli-Q water (Millipore, now Merck, https://www.merckmillipore.com) at an exact concentration of $2.35 \times 10^{-4}$ M, and this was used as the standard because it is absent in Arabidopsis (DeBolt *et al.*, 2006). Each sample was spiked with the standard solution as follows: approximately 150 mg of the sample was accurately weighed on an analytical balance (ML 54; Mettler Toledo, https://www.mt.com) to which about 10 mg of tartaric acid and 100 mg of acetonitrile were added by analytical weighing.

### Statistical analysis

All data evaluation and statistics were performed using PRISM 5.03 (GraphPad, https://www.graphpad.com).

## ACCESSION NUMBERS

The *A. thaliana frd3-7* T-DNA insertion (SALK_122235) is available from the Salk Collection. The RNA-Seq reads have been deposited in the National Center for Biotechnology Information (NCBI) Sequence Read Archive (SRA) Database with BioProject identification number PRJNA482933.

## ACKNOWLEDGEMENTS

We thank Prof. N. Verbruggen, Dr G. Vert and Dr S. Thomine for helpful discussions, and Dr S. Thiriet-Rupert for help with heat maps. We thank Dr C. Curie for the kind gift of *frd3-7* seeds. Funding was provided by the 'Fonds de la Recherche Scientifique–FNRS' (FRFC-2.4583.08, PDR-T.0206.13 and CDR J.0009.17). M.H. is Senior Research Associate of the F.R.S.-FNRS. M.S. is a doctoral fellow (F.R.I.A.).

## AUTHOR CONTRIBUTIONS

MH conceived and directed the research; MS conducted most experiments, with contributions from JS, and analyzed the data; MB and MS performed mass spectrometry analyses; EG contributed to the FTIR analyses; MC and BB contributed to ICP-AES analyses; MH and MS analyzed the RNA-Seq data; MH, PM and EDP supervised experiments; MS and MH wrote the article, with comments from all authors.

## CONFLICT OF INTEREST

No conflicts of interest to declare.

## SUPPORTING INFORMATION

Additional Supporting Information may be found in the online version of this article.

**Figure S1.** Impact of Zn on chlorophyll concentration in shoots.

**Figure S2.** Impact of Zn on shoot growth phenotypes.

**Figure S3.** Metal accumulation in shoots.

**Figure S4.** Effect of Zn on the ionome and Fe accumulation in roots in hydropony and in agar plate experiments.

**Figure S5.** Effect of the Zn/Fe ratio on the *frd3* phenotype.

**Figure S6.** Manganese toxicity phenotype.

**Figure S7.** Heat map of RNA-Seq data.

**Figure S8.** Root acidification activity.

**Figure S9.** Oxidative stress in roots.

**Figure S10.** PCA analysis of FTIR spectra in the 1300 and 900 $cm^{-1}$ range.

**Figure S11.** *NAS2* gene expression.

**Table S1.** Lists of differentially expressed genes from all pairwise comparisons described in Figure 4.

**Table S2.** Gene ontology enrichment analysis for pairwise comparisons described in Figure 4.

**Table S3.** Quantitative RT-PCR primer sequences and primer efficiencies.

### Open Research Badge

This article has earned an Open Data Badge for making publicly available the digitally-shareable data necessary to reproduce the reported results. The data is available at https://www.ncbi.nlm.nih.gov/bioproject/482933.

## REFERENCES

**Abadía, J., López-Millán, A.-F., Rombolà, A. and Abadía, A.** (2002) Organic acids and Fe deficiency: a review. *Plant Soil*, **241**, 75–86.

**Ali, M.B., Singh, N., Shohael, A.M., Hahn, E.J. and Paek, K.-Y.** (2006) Phenolics metabolism and lignin synthesis in root suspension cultures of *Panax ginseng* in response to copper stress. *Plant Sci.* **171**, 147–154.

**Alonso-Simón, A., García-Angulo, P., Mélida, H., Encina, A., Álvarez, J.M. and Acebes, J.L.** (2011) The use of FTIR spectroscopy to monitor modifications in plant cell wall architecture caused by cellulose biosynthesis inhibitors. *Plant Signal. Behav.* **6**, 1104–1110.

**Aznar, A., Chen, N.W.G., Rigault, M. *et al.*** (2014) Scavenging iron: a novel mechanism of plant immunity activation by microbial siderophores. *Plant Physiol.* **164**, 2167–2183.

**Baliardini, C., Meyer, C.-L., Salis, P., Saumitou-Laprade, P. and Verbruggen, N.** (2015) CATION EXCHANGER1 cosegregates with cadmium tolerance in the metal hyperaccumulator *Arabidopsis halleri* and plays a role in limiting oxidative stress in Arabidopsis Spp. *Plant Physiol.* **169**, 549–559.

**Bolger, A.M., Lohse, M. and Usadel, B.** (2014) Trimmomatic: a flexible trimmer for Illumina sequence data. *Bioinformatics*, **30**, 2114–2120.

**Bouzayen, M., Felix, G., Latché, A., Pech, J.-C. and Boller, T.** (1991) Iron: an essential cofactor for the conversion of 1-aminocyclopropane-1-carboxylic acid to ethylene. *Planta*, **184**, 244–247.

**Briat, J.-F., Dubos, C. and Gaymard, F.** (2015) Iron nutrition, biomass production, and plant product quality. *Trends Plant Sci.* **20**, 33–40.

**Broadley, M.R., White, P.J., Hammond, J.P., Zelko, I. and Lux, A.** (2007) Zinc in plants. *New Phytol.* **173**, 677–702.

**Brouquisse, R., Gaillard, J. and Douce, R.** (1986) Electron paramagnetic resonance characterization of membrane bound iron-sulfur clusters and aconitase in plant mitochondria. *Plant Physiol.* **81**, 247–252.

**Brumbarova, T., Bauer, P. and Ivanov, R.** (2015) Molecular mechanisms governing Arabidopsis iron uptake. *Trends Plant Sci.* **20**, 124–133.

**Chandran, D., Sharopova, N., Ivashuta, S., Gantt, J.S., VandenBosch, K.A. and Samac, D.A.** (2008) Transcriptome profiling identified novel genes associated with aluminum toxicity, resistance and tolerance in *Medicago truncatula*. *Planta*, **228**, 151–166.

**Charlier, J.B., Polese, C., Nouet, C., Carnol, M., Bosman, B., Kramer, U., Motte, P. and Hanikenne, M.** (2015) Zinc triggers a complex transcriptional and post-transcriptional regulation of the metal homeostasis gene *FRD3* in Arabidopsis relatives. *J Exp Bot.* **66**, 3865–3878.

**Chen, C-c, Chien, W.-F., Lin, N.-C. and Yeh, K.-C.** (2014) Alternative Functions of Arabidopsis YELLOW STRIPE-LIKE3: from metal translocation to pathogen defense. *PLoS ONE*, **9**, e98008.

**Colangelo, E.P. and Guerinot, M.L.** (2004) The essential basic helix-loop-helix protein FIT1 is required for the iron deficiency response. *Plant Cell.* **16**, 3400–3412.

**DeBolt, S., Cook, D.R. and Ford, C.M.** (2006) l-Tartaric acid synthesis from vitamin C in higher plants. *Proc. Natl. Acad. Sci. USA*, **103**, 5608–5613.

**Delhaize, E.** (1996) A metal-accumulator mutant of *Arabidopsis thaliana*. *Plant Physiol.* **111**, 849–855.

**Demirevska-Kepova, K., Simova-Stoilova, L., Stoyanova, Z., Hölzer, R. and Feller, U.** (2004) Biochemical changes in barley plants after excessive supply of copper and manganese. *Environ Exp Bot.* **52**, 253–266.

**Durrett, T.P., Gassmann, W. and Rogers, E.E.** (2007) The FRD3-mediated efflux of citrate into the root vasculature is necessary for efficient iron translocation. *Plant Physiol.* **144**, 197–205.

**Eide, D., Broderius, M., Fett, J. and Guerinot, M.L.** (1996) A novel iron-regulated metal transporter from plants identified by functional expression in yeast. *Proc. Natl. Acad. Sci. USA*, **93**, 5624–5628.

 

**Fourcroy, P., Sisó-Terraza, P., Sudre, D., Savirón, M., Reyt, G., Gaymard, F., Abadía, A., Abadia, J., Álvarez-Fernández, A. and Briat, J.-F.** (2014) Involvement of the ABCG37 transporter in secretion of scopoletin and derivatives by Arabidopsis roots in response to iron deficiency. *New Phytol.* **201**, 155–167.

**Fukao, Y., Ferjani, A., Tomioka, R., Nagasaki, N., Kurata, R., Nishimori, Y., Fujiwara, M. and Maeshima, M.** (2011) iTRAQ Analysis reveals mechanisms of growth defects due to excess zinc in Arabidopsis. *Plant Physiol.* **155**, 1893–1907.

**Gayomba, S.R., Zhai, Z., Jung, H-i and Vatamaniuk, O.K.** (2015) Local and systemic signaling of iron status and its interactions with homeostasis of other essential elements. *Front Plant Sci.* **6**, 716.

**Giles, K., Pringle, S.D., Worthington, K.R., Little, D., Wildgoose, J.L. and Bateman, R.H.** (2004) Applications of a travelling wave-based radio-frequency-only stacked ring ion guide. *Rapid Commun Mass Spectrom.* **18**, 2401–2414.

**Godbold, D.L., Horst, W.J., Marschner, H., Collins, J.C. and Thurman, D.A.** (1983) Root growth and Zn uptake by two ecotypes of *Deschampsia caespitosa* as affected by high Zn concentrations. *Z. Pflanzenphysiol.* **112**, 315–324.

**Godbold, D.L., Horst, W.J., Collins, J.C., Thurman, D.A. and Marschner, H.** (1984) Accumulation of zinc and organic acids in roots of zinc tolerant and non-tolerant ecotypes of *Deschampsia caespitosa*. *J. Plant Physiol.* **116**, 59–69.

**Goormaghtigh, E., Cabiaux, V. and Ruysschaert, J.-M.** (1994) Determination of Soluble and Membrane Protein Structure by Fourier Transform Infrared Spectroscopy. In *Physicochemical Methods in the Study of Biomembranes*. (Hilderson, H.J. and Ralston, G.B., eds). US, Boston, MA: Springer, pp. 405–450.

**Goormaghtigh, E., Raussens, V. and Ruysschaert, J.-M.** (1999) Attenuated total reflection infrared spectroscopy of proteins and lipids in biological membranes. *Biochim. Biophys. Act.* **1422**, 105–185.

**Green, L.S. and Rogers, E.E.** (2004) FRD3 controls iron localization in Arabidopsis. *Plant Physiol.* **136**, 2523–2531.

**Guerinot, M.L. and Yi, Y.** (1994) Iron: nutritious, noxious, and not readily available. *Plant Physiol.* **104**, 815–820.

**Hanikenne, M., Talke, I.N., Haydon, M.J., Lanz, C., Nolte, A., Motte, P., Kroymann, J., Weigel, D. and Kramer, U.** (2008) Evolution of metal hyperaccumulation required *cis*-regulatory changes and triplication of *HMA4*. *Nature*, **453**, 391–395.

**Hanikenne, M., Bernal, M. and Urzica, E.-I.** (2014) Ion homeostasis in the Chloroplast. In *Plastid Biology*. (Theg, S.M. and Wollman, F.-A., eds). New York, NY: Springer, pp. 465–514.

**Haydon, M.J. and Cobbett, C.S.** (2007) A novel major facilitator superfamily protein at the tonoplast influences zinc tolerance and accumulation in Arabidopsis. *Plant Physiol.* **143**, 1705–1719.

**Haydon, M.J. and Cobbett, C.S.** (2007) Transporters of ligands for essential metal ions in plants. *New Phytol.* **174**, 499–506.

**Haydon, M.J., Kawachi, M., Wirtz, M., Hillmer, S., Hell, R. and Kramer, U.** (2012) Vacuolar nicotianamine has critical and distinct roles under iron deficiency and for zinc sequestration in Arabidopsis. *Plant Cell*. **24**, 724–737.

**Hellemans, J., Mortier, G., De Paepe, A., Speleman, F. and Vandesompele, J.** (2007) qBase relative quantification framework and software for management and automated analysis of real-time quantitative PCR data. *Genome Biol.* **8**, R19.

**Irving, H.M.N.H. and Williams, R.J.P.** (1953) The stability of transition-metal complexes. *J. Chem. Soc.* 3192–3210.

**Ivanov, R., Brumbarova, T. and Bauer, P.** (2012) Fitting into the harsh reality: regulation of iron-deficiency responses in dicotyledonous plants. *Mol Plant*. **5**, 27–42.

**Jiang, X. and Wang, C.** (2008) Zinc distribution and zinc-binding forms in *Phragmites australis* under zinc pollution. *J. Plant Physiol.* **165**, 697–704.

**Johnson, R. and Wichern, D.** (2002) *Applied multivariate statistical analysis*. Saddle River, NJ: Prentice Hall.

**Jones, L., Milne, J.L., Ashford, D., McCann, M.C. and McQueen-Mason, S.J.** (2005) A conserved functional role of pectic polymers in stomatal guard cells from a range of plant species. *Planta*, **221**, 255–264.

**Kačuráková, M., Capek, P., Sasinková, V., Wellner, N., Ebringerová, A.** (2000) FT-IR study of plant cell wall model compounds: pectic polysaccharides and hemicelluloses. *Carbohyd. Polym.* **43**, 195–203.

**Kadota, Y., Shirasu, K. and Zipfel, C.** (2015) Regulation of the NADPH Oxidase RBOHD during plant immunity. *Plant Cell Physiol.* **56**, 1472–1480.

**Kieu, N.P., Aznar, A., Segond, D., Rigault, M., Simon-Côte, E., Kunz, C., Soulie, M.-C., Expert, D. and Dellagi, A.** (2012) Iron deficiency affects plant defence responses and confers resistance to *Dickeya dadantii* and *Botrytis cinerea*. *Mol Plant Pathol.* **13**, 816–827.

**Klatte, M., Schuler, M., Wirtz, M., Fink-Straube, C., Hell, R. and Bauer, P.** (2009) The analysis of Arabidopsis Nicotianamine Synthase mutants reveals functions for nicotianamine in seed iron loading and iron deficiency responses. *Plant Physiol.* **150**, 257–271.

**Kobayashi, T. and Nishizawa, N.** (2012) Iron uptake, translocation, and regulation in higher plants. *Annu. Rev. Plant. Biol.* **63**, 131–152.

**Koen, E., Trapet, P., Brulé, D. *et al.*** (2014) β-Aminobutyric acid (BABA)-induced resistance in *Arabidopsis thaliana*: link with iron homeostasis. *Mol. Plant Microbe Interact.* **27**, 1226–1240.

**Krämer, U., Talke, I.N. and Hanikenne, M.** (2007) Transition metal transport. *FEBS Lett.* **581**, 2263–2272.

**Krzesłowska, M.** (2011) The cell wall in plant cell response to trace metals: polysaccharide remodeling and its role in defense strategy. *Acta Physiol. Plant.* **33**, 35–51.

**Le Gall, H., Philippe, F., Domon, J.-M., Gillet, F., Pelloux, J. and Rayon, C.** (2015) Cell wall metabolism in response to Abiotic Stress. *Plants*, **4**, 112.

**Lei, Y., Korpelainen, H. and Li, C.** (2007) Physiological and biochemical responses to high Mn concentrations in two contrasting *Populus cathayana* populations. *Chemosphere*, **68**, 686–694.

**Lequeux, H., Hermans, C., Lutts, S. and Verbruggen, N.** (2010) Response to copper excess in *Arabidopsis thaliana*: impact on the root system architecture, hormone distribution, lignin accumulation and mineral profile. *Plant Physiol. Biochem.* **48**, 673–682.

**Levine, A., Tenhaken, R., Dixon, R. and Lamb, C.** (1994) H2O2 from the oxidative burst orchestrates the plant hypersensitive disease resistance response. *Cell*, **79**, 583–593.

**Li, J., Wu, X.-D., Hao, S.-T., Wang, X.-J. and Ling, H.-Q.** (2008) Proteomic response to iron deficiency in tomato root. *Proteomics*, **8**, 2299–2311.

**Li, X., Zhang, H., Ai, Q., Liang, G. and Yu, D.** (2016) Two bHLH Transcription factors, bHLH34 and bHLH104, regulate iron homeostasis in *Arabidopsis thaliana*. *Plant Physiol.* **170**, 2478–2493.

**Lichtenthaler, H.K. and Buschmann, C.** (2001) Chlorophylls and carotenoids: measurement and characterization by UV-VIS spectroscopy. *Current Protocols in Food Analytical Chemistry*, **1**, F4.3.1–F4.3.8.

**Liu, G., Greenshields, D.L., Sammynaiken, R., Hirji, R.N., Selvaraj, G. and Wei, Y.** (2007) Targeted alterations in iron homeostasis underlie plant defense responses. *J Cell Sci.* **120**, 596–605.

**Long, T.A., Tsukagoshi, H., Busch, W., Lahner, B., Salt, D.E. and Benfey, P.N.** (2010) The bHLH transcription factor POPEYE regulates response to iron deficiency in Arabidopsis roots. *Plant Cell.* **22**, 2219–2236.

**Love, M.I., Huber, W. and Anders, S.** (2014) Moderated estimation of fold change and dispersion for RNA-seq data with DESeq2. *Genome Biol.* **15**, 550.

**Mai, H.-J., Pateyron, S. and Bauer, P.** (2016) Iron homeostasis in *Arabidopsis thaliana*: transcriptomic analyses reveal novel FIT-regulated genes, iron deficiency marker genes and functional gene networks. *BMC Plant Biol.* **16**, 211.

**Marschner, H. and Marschner, P.** (2012) *Marschner's Mineral Nutrition of Higher Plants*. Academic Press.

**Mendoza-Cózatl, D.G., Xie, Q., Akmakjian, G.Z. *et al.*** (2014) OPT3 is a component of the iron-signaling network between leaves and roots and misregulation of OPT3 leads to an over-accumulation of cadmium in seeds. *Mol. Plant.* **7**, 1455–1469.

**Meyer, C.-L., Juraniec, M., Huguet, S., Chaves-Rodriguez, E., Salis, P., Isaure, M.-P., Goormaghtigh, E. and Verbruggen, N.** (2015) Intraspecific variability of cadmium tolerance and accumulation, and cadmium-induced cell wall modifications in the metal hyperaccumulator *Arabidopsis halleri*. *J. Exp. Bot.* **66**, 3215–3227.

**Millaleo, R., Reyes-Díaz, M., Alberdi, M., Ivanov, A.G., Krol, M. and Hüner, N.P.A.** (2013) Excess manganese differentially inhibits photosystem I versus II in *Arabidopsis thaliana*. *J. Exp. Bot.* **64**, 343–354.

**Morrissey, J., Baxter, I.R., Lee, J., Li, L., Lahner, B., Grotz, N., Kaplan, J., Salt, D.E. and Guerinot, M.L.** (2009) The Ferroportin metal efflux proteins function in iron and Cobalt homeostasis in Arabidopsis. *Plant Cell.* **21**, 3326–3338.

**Moura, J.C.M.S., Bonine, C.A.V., De Oliveira, F.V.J., Dornelas, M.C. and Mazzafera, P.** (2010) Abiotic and biotic stresses and changes in the lignin content and composition in plants. *J. Integr. Plant Biol.* **52**, 360–376.

**Muschitz, A., Riou, C., Mollet, J.-C., Gloaguen, V. and Faugeron, C.** (2015) Modifications of cell wall pectin in tomato cell suspension in response to cadmium and zinc. *Acta Physiol. Plant.* **37**, 245.

**Nouet, C., Motte, P. and Hanikenne, M.** (2011) Chloroplastic and mitochondrial metal homeostasis. *Trends Plant Sci.* **16**, 395–404.

**Nouet, C., Charlier, J.-B., Carnol, M., Bosman, B., Farnir, F., Motte, P. and Hanikenne, M.** (2015) Functional analysis of the three *HMA4* copies of the metal hyperaccumulator *Arabidopsis halleri*. *J. Exp. Bot.* **66**, 5783–5795.

**Palmer, C.M. and Guerinot, M.L.** (2009) Facing the challenges of Cu, Fe and Zn homeostasis in plants. *Nat. Chem. Biol.* **5**, 333–340.

**Palmer, C.M., Hindt, M.N., Schmidt, H., Clemens, S. and Guerinot, M.L.** (2013) MYB10 and MYB72 are required for growth under iron-limiting conditions. *PLoS Genet.* **9**, e1003953.

**Pierre, J.L. and Fontecave, M.** (1999) Iron and activated oxygen species in biology: the basic chemistry. *Biometals*, **12**, 195–199.

**Pineau, C., Loubet, S., Lefoulon, C., Chalies, C., Fizames, C., Lacombe, B., Ferrand, M., Loudet, O., Berthomieu, P. and Richard, O.** (2012) Natural variation at the *FRD3* MATE transporter locus reveals cross-talk between Fe homeostasis and Zn tolerance in *Arabidopsis thaliana*. *PLoS Genet.* **8**, e1003120.

**Piterková, J., Luhová, L., Mieslerová, B., Lebeda, A. and Petřivalský, M.** (2013) Nitric oxide and reactive oxygen species regulate the accumulation of heat shock proteins in tomato leaves in response to heat shock and pathogen infection. *Plant Sci.* **207**, 57–65.

**Pringle, S.D., Giles, K., Wildgoose, J.L., Williams, J.P., Slade, S.E., Thalassinos, K., Bateman, R.H., Bowers, M.T. and Scrivens, J.H.** (2007) An investigation of the mobility separation of some peptide and protein ions using a new hybrid quadrupole/travelling wave IMS/oa-ToF instrument. *Int. J. Mass Spectrom.* **261**, 1–12.

**Ranieri, A., Castagna, A., Pacini, J., Baldan, B., Mensuali Sodi, A. and Soldatini, G.F.** (2003) Early production and scavenging of hydrogen peroxide in the apoplast of sunflower plants exposed to ozone. *J. Exp. Bot.* **54**, 2529–2540.

**Rellán-Álvarez, R., Giner-Martínez-Sierra, J., Orduna, J., Orera, I., Rodríguez-Castrillón, J.Á., García-Alonso, J.I., Abadía, J. and Álvarez-Fernández, A.** (2010) Identification of a tri-iron(III), tri-citrate complex in the xylem sap of iron-deficient tomato resupplied with iron: new insights into plant iron long-distance transport. *Plant Cell Physiol.* **51**, 91–102.

**Robinson, N.J., Procter, C.M., Connolly, E.L. and Guerinot, M.L.** (1999) A ferric-chelate reductase for iron uptake from soils. *Nature*, **397**, 694–697.

**Rodríguez-Celma, J., Pan, I., Li, W., Lan, P., Buckhout, T. and Schmidt, W.** (2013) The transcriptional response of Arabidopsis leaves to Fe deficiency. *Front Plant Sci.* **4**, 276.

**Rodríguez-Celma, J., Connorton, J.M., Kruse, I., Green, R.T., Franceschetti, M., Chen, Y.-T., Cui, Y., Ling, H.-Q., Yeh, K.-C. and Balk, J.** (2019) Arabidopsis BRUTUS-LIKE E3 ligases negatively regulate iron uptake by targeting transcription factor FIT for recycling. *Proc. Natl. Acad. Sci.* **116**, 17584–17591.

**Rogers, E.E. and Guerinot, M.L.** (2002) FRD3, a member of the multidrug and toxin efflux family, controls iron deficiency responses in Arabidopsis. *Plant Cell.* **14**, 1787–1799.

**Romera, F.J., García, M.J., Lucena, C., Martínez-Medina, A., Aparicio, M.A., Ramos, J., Alcántara, E., Angulo, M. and Pérez-Vicente, R.** (2019) Induced systemic resistance (ISR) and Fe deficiency responses in dicot plants. *Front. Plant Sci.* **10**.

**Römheld, V.** (1987) Different strategies for iron acquisition in higher plants. *Physiol Plant.* **70**, 231–234.

**Roschzttardtz, H., Conejero, G., Curie, C. and Mari, S.** (2009) Identification of the endodermal vacuole as the iron storage compartment in the arabidopsis embryo. *Plant Physiol.* **151**, 1329–1338.

**Roschzttardtz, H., Séguéla-Arnaud, M., Briat, J.-F., Vert, G. and Curie, C.** (2011) The FRD3 citrate effluxer promotes iron nutrition between symplastically disconnected tissues throughout arabidopsis development. *Plant Cell*, **23**, 2725–2737.

**Ruijter, J.M., Ramakers, C., Hoogaars, W.M.H., Karlen, Y., Bakker, O., van den Hoff, M.J.B. and Moorman, A.F.M.** (2009) Amplification efficiency: linking baseline and bias in the analysis of quantitative PCR data. *Nucleic Acids Res.* **37**, e45–e45.

**Santi, S. and Schmidt, W.** (2009) Dissecting iron deficiency-induced proton extrusion in Arabidopsis roots. *New Phytol.* **183**, 1072–1084.

**Schaaf, G., Honsbein, A., Meda, A.R., Kirchner, S., Wipf, D. and von Wirén, N.** (2006) AtIREG2 encodes a tonoplast transport protein involved in iron-dependent nickel detoxification in *Arabidopsis thaliana* roots. *J. Biol. Chem.* **281**, 25532–25540.

**Schmid, W.E., Haag, H.P. and Epstein, E.** (1965) Absorption of Zinc by excised barley roots. *Physiol Plant.* **18**, 860–869.

**Schmidt, W.** (1999) Mechanisms and regulation of reduction-based iron uptake in plants. *New Phytol.* **141**, 1–26.

**Schmidt, W.** (2003) Iron solutions: acquisition strategies and signaling pathways in plants. *Trends Plant Sci.* **8**, 188–193.

**Schmidt, H., Günther, C., Weber, M., Spörlein, C., Loscher, S., Böttcher, C., Schobert, R. and Clemens, S.** (2014) Metabolome analysis of *arabidopsis thaliana* roots identifies a key metabolic pathway for iron acquisition. *PLoS ONE*, **9**, e102444.

**Schuler, M., Keller, A., Backes, C., Philippar, K., Lenhof, H.-P. and Bauer, P.** (2011) Transcriptome analysis by GeneTrail revealed regulation of functional categories in response to alterations of iron homeostasis in *Arabidopsis thaliana*. *BMC Plant Biol.* **11**, 87.

**Schvartzman, M.S., Corso, M., Fataftah, N., Scheepers, M., Nouet, C., Bosman, B., Carnol, M., Motte, P., Verbruggen, N. and Hanikenne, M.** (2018) Adaptation to high zinc depends on distinct mechanisms in metallicolous populations of *Arabidopsis halleri*. *New Phytol.* **218**, 269–282.

**Segond, D., Dellagi, A., Lanquar, V., Rigault, M., Patrit, O., Thomine, S. and Expert, D.** (2009) NRAMP genes function in *Arabidopsis thaliana* resistance to *Erwinia chrysanthemi* infection. *Plant J.* **58**, 195–207.

**Séguéla, M., Briat, J.-F., Vert, G. and Curie, C.** (2008) Cytokinins negatively regulate the root iron uptake machinery in Arabidopsis through a growth-dependent pathway. *Plant J.* **55**, 289–300.

**Sene, C., McCann, M.C., Wilson, R.H. and Grinter, R.** (1994) Fourier-Transform raman and fourier-transform infrared spectroscopy (an investigation of five higher plant cell walls and their components). *Plant Physiol.* **106**, 1623–1631.

**Shanmugam, V., Lo, J.C., Wu, C.L., Wang, S.L., Lai, C.C., Connolly, E.L., Huang, J.L. and Yeh, K.C.** (2011) Differential expression and regulation of iron-regulated metal transporters in Arabidopsis halleri and Arabidopsis thaliana–the role in zinc tolerance. *New Phytol.* **190**, 125–137.

**Shanmugam, V., Tsednee, M. and Yeh, K.-C.** (2012) ZINC TOLERANCE INDUCED BY IRON 1 reveals the importance of glutathione in the cross-homeostasis between zinc and iron in *Arabidopsis thaliana*. *Plant J.* **69**, 1006–1017.

**Shvartsburg, A.A.** (2008) *Differential Ion Mobility Spectrometry: Nonlinear Ion Transport and Fundamentals of FAIMS*. CRC Press.

**Shvartsburg, A.A. and Smith, R.D.** (2008) Fundamentals of traveling wave ion mobility spectrometry. *Anal Chem.* **80**, 9689–9699.

**Sinclair, S.A., Sherson, S.M., Jarvis, R., Camakaris, J. and Cobbett, C.S.** (2007) The use of the zinc-fluorophore, Zinpyr-1, in the study of zinc homeostasis in Arabidopsis roots. *New Phytol.* **174**, 39–45.

**Sivitz, A., Hermand, V., Curie, C. and Vert, G.** (2012) Arabidopsis bHLH100 and bHLH101 control iron homeostasis via a FIT-independent pathway. *PLoS ONE*, **7**, e44843.

**Stephan, U.W. and Scholz, G.** (1993) Nicotianamine: mediator of transport of iron and heavy metals in the phloem? *Physiol Plant.* **88**, 522–529.

**Stohs, S.J. and Bagchi, D.** (1995) Oxidative mechanisms in the toxicity of metal ions. *Free Radic. Biol. Med.* **18**, 321–336.

**Suzuki, N. and Katano, K.** (2018) Coordination between ROS regulatory systems and other pathways under heat stress and pathogen attack. *Front Plant Sci.* **9**, 490.

**Takahashi, M., Terada, Y., Nakai, I., Nakanishi, H., Yoshimura, E., Mori, S. and Nishizawa, N.K.** (2003) Role of nicotianamine in the intracellular delivery of metals and plant reproductive development. *Plant Cell.* **15**, 1263–1280.

**Talke, I.N., Hanikenne, M. and Kramer, U.** (2006) Zinc-dependent global transcriptional control, transcriptional deregulation, and higher gene copy number for genes in metal homeostasis of the hyperaccumulator *Arabidopsis halleri*. *Plant Physiol.* **142**, 148–167.

 

**Tillemans, V., Leponce, I., Rausin, G., Dispa, L. and Motte, P.** (2006) Insights into nuclear organization in plants as revealed by the dynamic distribution of arabidopsis SR splicing factors. *Plant Cell.* **18**, 3218–3234.

**Torres, M.A., Jones, J.D.G. and Dangl, J.L.** (2006) Reactive oxygen species signaling in response to pathogens. *Plant Physiol.* **141**, 373–378.

**Turner, R.G.** (1970) The subcelluar distribution of zinc and copper within the roots of metal-tolerant clones of *Agrostis tenuis Sibth*. *New Phytol.* **69**, 725–731.

**Turner, R.G. and Marshall, C.** (1972) The Accumulation of Zinc by Subcellular Fractions of Roots of *Agrostis tenuis Sibth*. In Relation to Zinc Tolerance. *New Phytol.* **71**, 671–676.

**Vandesompele, J., De Preter, K., Pattyn, F., Poppe, B., Van Roy, N., De Paepe, A. and Speleman, F.** (2002) Accurate normalization of real-time quantitative RT-PCR data by geometric averaging of multiple internal control genes. *Genome Biol.* **3**, research0034.0031.

**Verbon, E.H., Trapet, P.L., Stringlis, I.A., Kruijs, S., Bakker, P.A.H.M. and Pieterse, C.M.J.** (2017) Iron and Immunity. *Ann. Rev. Phythopathol.* **55**, 355–375.

**Vert, G., Grotz, N., Dedaldechamp, F., Gaymard, F., Guerinot, M.L., Briat, J.F. and Curie, C.** (2002) IRT1, an Arabidopsis transporter essential for iron uptake from the soil and for plant growth. *Plant Cell.* **14**, 1223–1233.

**de Vos, C.R., Lubberding, H.J. and Bienfait, H.F.** (1986) Rhizosphere acidification as a response to iron deficiency in bean plants. *Plant Physiol.* **81**, 842–846.

**Walker, E.L. and Connolly, E.L.** (2008) Time to pump iron: iron-deficiency-signaling mechanisms of higher plants. *Curr. Opin. Plant Biol.* **11**, 530–535.

**von Wirén, N., Klair, S., Bansal, S., Briat, J.F., Khodr, H., Shioiri, T., Leigh, R.A. and Hider, R.C.** (1999) Nicotianamine chelates both FeIII and FeII. Implications for metal transport in plants. *Plant Physiol.* **119**, 1107–1114.

**Ye, Y.Q., Jin, C.W., Fan, S.K., Mao, Q.Q., Sun, C.L., Yu, Y. and Lin, X.Y.** (2015) Elevation of NO production increases Fe immobilization in the Fe-deficiency roots apoplast by decreasing pectin methylation of cell wall. *Sci. Rep.* **5**, 10746.

**Yi, Y. and Guerinot, M.** (1996) Genetic evidence that induction of root Fe(III) chelate reductase activity is necessary for iron uptake under iron deficiency. *Plant J.* **10**, 835–844.

**Yuan, Y., Zhang, J., Wang, D. and Ling, H.** (2005) AtbHLH29 of *Arabidopsis thaliana* is a functional ortholog of tomato FER involved in controlling iron acquisition in strategy I plants. *Cell Res.* **15**, 613–621.

**Yuan, Y., Wu, H., Wang, N., Li, J., Zhao, W., Du, J., Wang, D. and Ling, H.Q.** (2008) FIT interacts with AtbHLH38 and AtbHLH39 in regulating iron uptake gene expression for iron homeostasis in Arabidopsis. *Cell Res.* **18**, 385–397.

**Wintermans, J.F.G.M. and De Mots, A.** (1965) Spectrophotometric characteristics of chlorophylls a and b and their phenophytins in ethanol. *Biochim Biophys Acta*, **109**, 448–453.

**Zamioudis, C., Hanson, J. and Pieterse Corné, M.J.** (2014) β-Glucosidase BGLU42 is a MYB72-dependent key regulator of rhizobacteria-induced systemic resistance and modulates iron deficiency responses in Arabidopsis roots. *New Phytol.* **204**, 368–379.

**Zamioudis, C., Korteland, J., Van Pelt, J.A. *et al.*** (2015) Rhizobacterial volatiles and photosynthesis-related signals coordinate MYB72 expression in Arabidopsis roots during onset of induced systemic resistance and iron-deficiency responses. *Plant J.* **84**, 309–322.

**Zornoza, P., Vázquez, S., Esteban, E., Fernández-Pascual, M. and Carpena, R.** (2002) Cadmium-stress in nodulated white lupin: strategies to avoid toxicity. *Plant Physiol. Biochem.* **40**, 1003–1009.